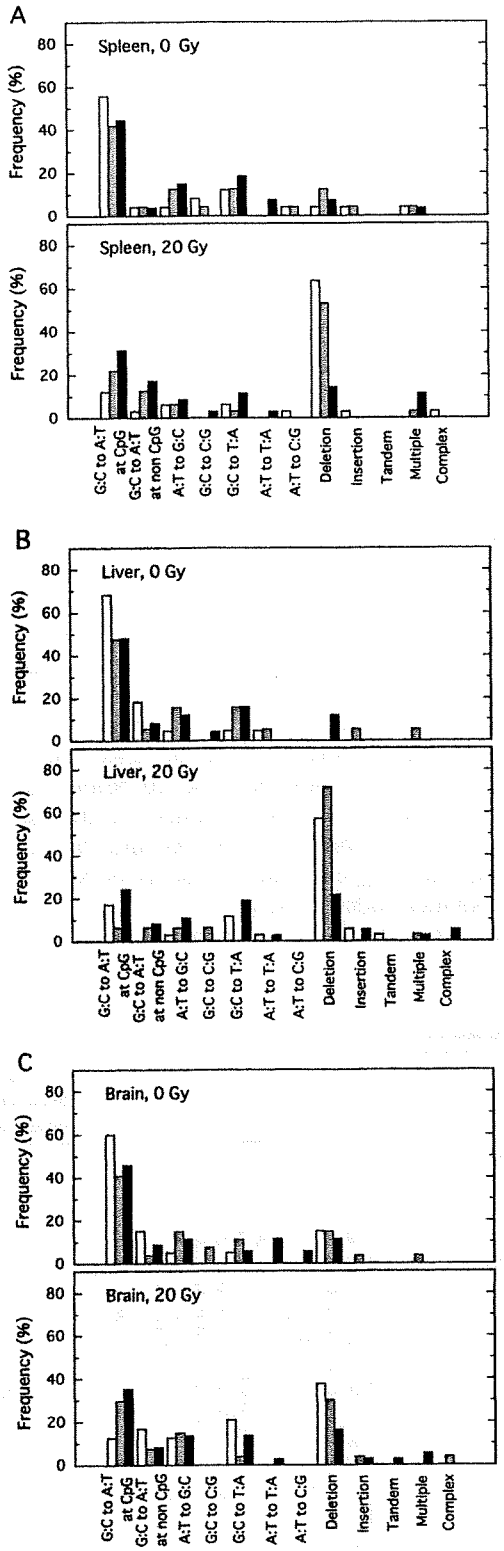

FIG. 2. Mutation spectra in nonirradiated and 20 Gy-irradiated *Ku70*$^{+/+}$, $^{+/-}$ and $^{-/-}$ *lacZ* transgenic mice 3.5 days postirradiation. The frequencies of different types of mutations revealed by sequencing of mutant clones are shown. Open, gray and black columns represent wild-type mice, *Ku70*$^{+/-}$ mice and *Ku70*$^{-/-}$ mice, respectively. Deletion-type mutations were induced by irradiation of *Ku70*$^{+/+}$ and $^{+/-}$ mice, but they were not prominent in $^{-/-}$ mice.

ficient mice and 109 in irradiated *Ku70*-deficient mice. Fisher's exact probability test showed that the number of multiple mutations appearing separately at a distance of more than 558 bp was significantly higher in *Ku70*$^{-/-}$ mice (4/109) than in *Ku70*-proficient mice (0/188, $P = 0.0175$).

DNA Breaks and Rejoining

The suppression of radiation-induced mutation in *Ku70*-deficient mice could be explained by lack of rejoining of DNA double-strand breaks, which would not be detected as mutations, or by repair through homologous recombination, which is known to be error-free. To obtain more information, we analyzed DNA breaks and phosphorylated H2AX, which is supposed to be associated with free ends of double-strand breaks.

SFGE was adopted to assess DNA double-strand breaks and their rejoining. With this approach, the amount of DNA breaks is estimated as the DNA released from a well into the gel after electrophoresis. The fraction of released DNA was shown to increase with radiation dose (*31*). As is indicated in Fig. 3A, immediately after exposure to 20 Gy, the amount of fragmented DNA released from the well showed an increase in all tissues of all genotypes compared to nonirradiated mice. However, 3.5 days after irradiation, the amount of fragmented DNA showed genotype- and tissue-specific differences. Fragmented DNA was much reduced in all three tissues of *Ku70*$^{+/-}$ mice. In *Ku70*$^{-/-}$ mice, on the other hand, a significant amount of DNA remained fragmented, showing suppression of DNA rejoining (Fig. 3). The statistical analysis comparing the amounts of fragmented DNAs in *Ku70*-deficient mouse tissues immediately and 3.5 days after 20 Gy irradiation showed that the rejoining was significant in liver ($P = 0.00877$) and brain ($P = 0.0104$) but not in spleen ($P = 0.0734$). This indicates that some DNA rejoining took place in the absence of *Ku70* but not as much as that observed in *Ku70*-proficient mice.

The presence of unrepaired DNA breaks in irradiated *Ku70*$^{-/-}$ mice was further indicated by the persistent presence of phosphorylated histone H2AX at 3.5 days postirradiation. Figure 4 shows Western blots of phosphorylated H2AX (γ-H2AX) in spleen, liver and brain at 1 h and 3.5 days after irradiation. In *Ku70*$^{+/-}$ mice, the γ-H2AX band observed at 1 h after irradiation disappeared at 3.5 days, whereas *Ku70*$^{-/-}$ mice showed significant levels of γ-H2AX at 3.5 days postirradiation, suggesting the persistent presence of unrepaired DNA breaks.

DISCUSSION

Double-strand breaks are considered to be the most important damage induced by ionizing radiation. Other types of lesions such as base damage and single-strand breaks, although more common, are repaired rapidly and do not have such disastrous consequences for cells if they are misrepaired, because they do not generally involve the loss of

TABLE 1
The Number of Deletion Mutations of Different Sizes Found in the Three Tissues

		Control			20 Gy		
Tissue	*Ku70*	Total mutations[a]	1–50 bp[b]	>50 bp[c]	Total mutations[a]	1–50 bp[b]	>50 bp[c]
Spleen	+/+, +/−	69	4 (5.8)[d]	0	64	34 (53.1)	4 (6.3)
	−/−	27	2 (7.4)	0	35	2 (5.7)	3 (8.6)
Liver	+/+, +/−	41	0	0	73	40 (54.8)	1 (1.4)
	−/−	25	3 (12.0)	0	37	5 (13.5)	3 (8.1)
Brain	+/+, +/−	47	7 (14.9)	0	51	15 (29.4)	1 (2.0)
	−/−	35	2 (5.7)	0	37	3 (8.1)	3 (8.1)

[a] Total number of independent mutations found.
[b] Number of deletion mutations of 1 to 50 bp.
[c] Number of deletion mutations of more than 50 bp.
[d] The numbers in parentheses indicate percentages.

DNA sequences from the genome. The present study demonstrates that NHEJ of DNA double-strand breaks is the major source of radiation-induced mutagenesis in mouse tissues. Double-strand breaks are only a minor component (about 1/250) of the total DNA damage (*34*). Since most of the radiation-induced mutations are suppressed in *Ku70*$^{-/-}$ mice (Fig. 1), it would appear that most DNA damage other than double-strand breaks is repaired correctly. It should be noted that a small number of mutations were induced in Ku70-deficient mice. These could be the result of mistakes in the other repair processes such as translesional DNA synthesis on damaged bases.

The number of DNA double-strand breaks induced by 1 Gy of radiation is estimated to be about 30 per cell with approximately 6×10^9 bp of total DNA (*34, 35*). The number of double-strand breaks induced in the 3.1-kbp-long *lacZ* gene by 20 Gy radiation would be estimated to be 30×10^{-5} ($30 \times 20 \times 3.1 \times 10^3/6 \times 10^9$). Since the number of radiation-induced mutations in the tissues is $23–32 \times 10^{-5}$ (Fig. 1), the two numbers are similar. This suggests that each double-strand break in the *lacZ* gene leads to one mutation. This is reasonable because most radiation-induced double-strand breaks are accompanied by chemical alterations in one or more bases or the deoxyribose at the broken ends, and they must be removed before the break is sealed. In other words, the closeness of the estimated number of DNA double-strand breaks and the measured mutant frequency suggests that the fidelity of NHEJ is very poor for radiation-induced breaks.

One point that should be remembered in the interpreta-

TABLE 2
Multiple and Complex Type Mutations

Ku70	Dose (Gy)	Tissue	ID	Type[a]	Position[b]	Change[c]	Distance between the mutations (bp)
+/+	20	Spleen	M1-12	Multiple (−3, −1)	1456–1458, 1461	A T C C T T C C C G C → A T · · · T C C · G C	3
+/−	20	Liver	M1-16	Multiple (BS, BS)	2906	C A G T C → C A T T C	14
					2921	G A T G G → G A A G G	
		Brain	F2-10	Complex (−2, +1)	2351–2352	C C G C C G → C C T C G	—
−/−	0	Spleen	F2-7	Multiple (BS, BS, BS)	1111	G T C A G → G T T A G	11, 1
					1123, 1125	A T G A G C A → A T A A A C A	
	20	Spleen	M2-12	Multiple (BS, BS)	1187	T T C G C → T T T G C	993
					2181	C G T C T → C G C C T	
			M3-16	Multiple (BS, BS)	2392	A C G A C → A C A A C	558
					2951	C G C G G → C G T G G	
			M3-17	Multiple (BS, BS)	20	T T C A C → T T T A C	116
					1187	T T C G C → T T T G C	
		Liver	M2-16	Multiple (BS, BS)	452, 454	T G G C G T T → T G T C T T T	1
			F3-13	Complex (−1, +2)	881	T C G C T → T C A T C T	—
			F3-17	Multiple (BS, BS, +1)	1369, 1370, 1372	A C C C G A G T → A C A A G A A G T	2
		Brain	M3-4	Multiple (BS, BS)	154	A T C G C → A T T G C	1041
					1196	T C C G A → T C T G A	

[a] BS; base substitution, negative number; deletion, positive number; insertion.
[b] The position of nucleotide is numbered from the first nucleotide of initiation codon of the *lacZ* gene.
[c] The nucleotides showing alteration are underlined. The deleted nucleotides are shown by dots.

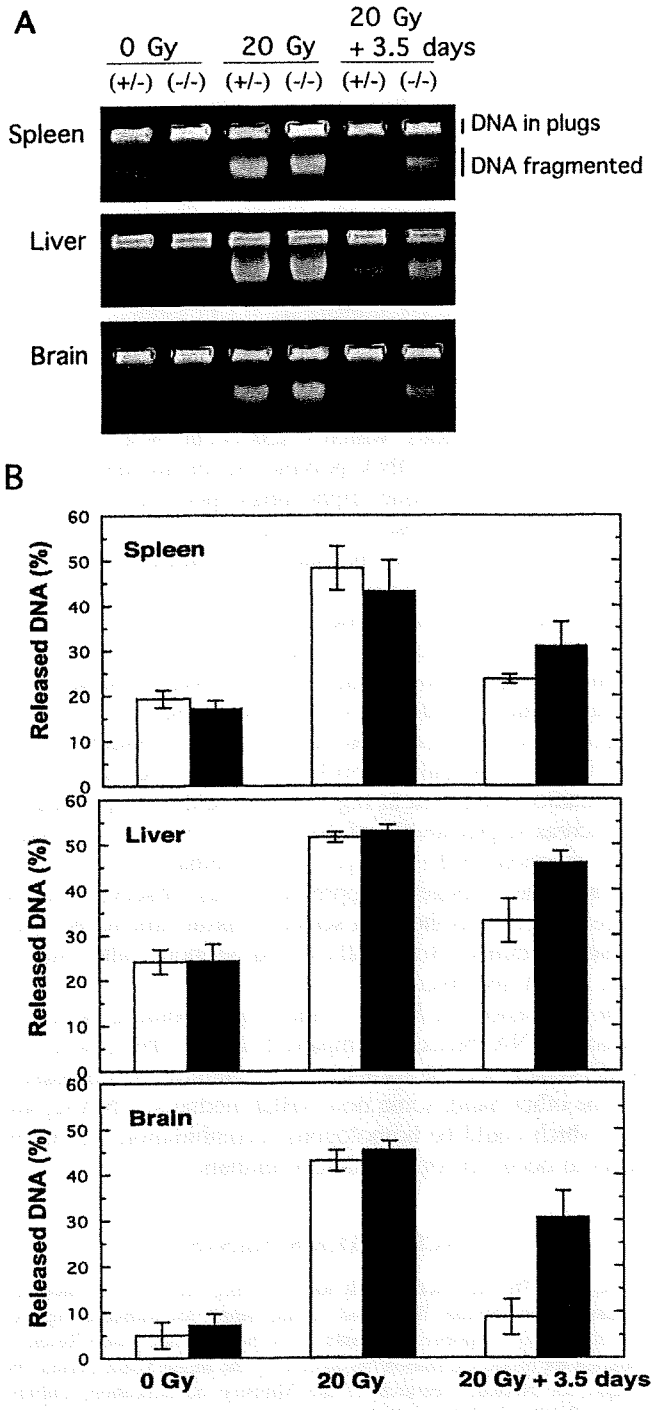

FIG. 3. SFGE analyses of DNA breaks and rejoining after 20 Gy of irradiation in *Ku70*-proficient $^{+/-}$ and deficient $^{-/-}$ mice. Panel A: Irradiation with 20 Gy increased the fraction of fragmented DNA which was released from the well in both *Ku70*$^{+/-}$ and $^{-/-}$ mice. At 3.5 days after irradiation, the fragmented DNA was reduced to the levels found in non-irradiated tissues in *Ku70*$^{+/-}$ mice and to intermediate levels in *Ku70*$^{-/-}$ mice. A similar trend was observed in the three tissues examined. Panel B: The experiment was repeated three times and the percentage of the fragmented DNA was quantified. The averages and standard deviations are shown. White columns represent *Ku70*$^{+/-}$ mice and the black columns *Ku70*$^{-/-}$ mice.

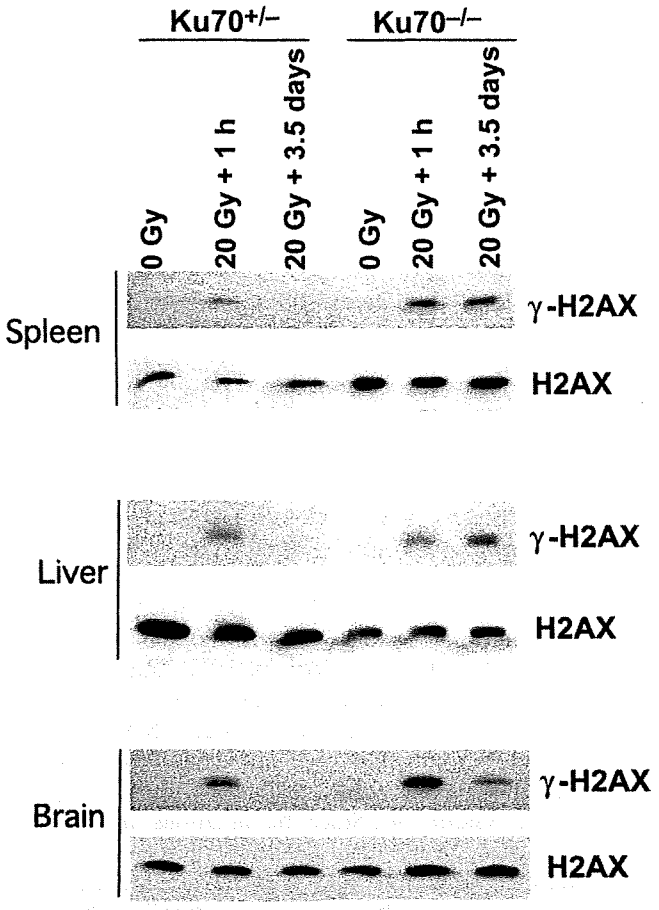

FIG. 4. Western blot analysis of the phosphorylation of histone H2AX. In *Ku70*-proficient mice, the phosphorylated H2AX (γ-H2AX) band was present at one hour after irradiation (20 Gy) and disappeared at 3.5 days in all tissues. In *Ku70*$^{-/-}$ mice, however, the γ-H2AX remained positive at 3.5 days after irradiation, suggesting that many of the radiation-induced DNA breaks remain unrepaired.

tion of the present results is that the mutational changes observed are limited to events within the 3.1-kbp-long *lacZ* gene. Therefore, large rearrangements such as deletions of more than a few kbp of DNA or translocation of the *lacZ* gene to the other chromosome cannot be detected in the present assay system, because each *lacZ* gene retrieved from the mouse genome needs to be packed into a λ phage to be analyzed for mutations. Thus the assay can monitor only base substitutions and deletions/insertions of up to a few kbp within or including the *lacZ* gene.

The other point to be noted is that the doses used in the present study are 20 Gy and 50 Gy. Although liver and brain tissue did not show any appreciable alterations after irradiation with those doses, the spleen was significantly smaller 3.5 days after irradiation. This is in accord with the prevalence of cell death in the spleen within 24 h after irradiation (*36*). Thus the data for spleen at 3.5 days after irradiation must represent the survival of only a minor fraction of spleen cells after these high doses. Further, defi-

ciency of Ku80, the other key protein of NHEJ, has been shown to enhance apoptosis in the spleen after irradiation (*36*). Thus it is possible that the reduction of radiation-induced mutations in the spleen of NHEJ-deficient mice reflects the preferential elimination of cells harboring a *lacZ* mutation. However, this is not likely, because it is difficult to imagine that the apoptosis induction system can work preferentially on cells that have damage or mutation on the *lacZ* gene. After irradiation with 20 Gy, each cell suffers significant DNA damage, including approximately 600 double-strand breaks, and no cell will be free of damage. The cells that have damage on the *lacZ* gene must have many other lesions on the other part of the genome. Under these conditions, it would be difficult to recognize selectively the cells containing damage in the *lacZ* gene. In addition, the *lacZ* gene used in the system does not have the promoter needed for transcription in mouse cells. Hence it is not expressed and could not be subject to selection by the cellular apoptosis system whether the gene is mutated or not.

Rothkamm *et al.* examined DNA ligation in cultured cells using pulsed-field gel electrophoresis and found that 50% of the double-strand breaks induced by an acute high dose of radiation (80 Gy) resulted in large DNA rearrangements, probably by ligation of illegitimate ends by NHEJ. The other 50% were ligated accurately without using the NHEJ repair system (*14*). Since the mutations monitored in the present study were small deletions of less than a few kbp within the *lacZ* gene, they must have belonged to the category considered to be "accurate ligation" in the study of Rothkamm *et al.* (*14*). At present, there is no way to estimate the ratio of mutation-free ligation and mutation-linked ligation in the "accurate ligation".

Our study as well as that of Rothkamm *et al.* (*14*) supports the existence of a functional double-strand break repair system other than NHEJ, because significant levels of DNA rejoining were observed after irradiation in NHEJ-deficient tissues and cells. It could be homologous recombination (HR) repair that functions as a form of error-free double-strand break repair when homologous DNA sequences are present. The strong repression of mutation induction in *Ku70*-deficient mouse tissues supports the importance of HR in these cells. It is also possible that microhomology-mediated end joining (MMEJ), which is error-prone and is suggested to be distinct from NHEJ (*3*), may function in NHEJ-deficient cells. Repair by MMEJ has been reported to result in relatively large deletions with short repeat sequences at the ends of deleted fragment (*3*). The frequency of repeated sequences at the ends of deleted DNA, a hallmark of MMEJ, was similar in both wild-type and *Ku70*-deficient mice (data not shown), which does not support a role for MMEJ. However, the deletion mutations observed in irradiated *Ku70*-deficient mice appear to contain slightly larger deletions than those in *Ku70*-proficient irradiated mice (Table 1), which may support the latter idea.

In the present study, we found nine multiple mutations (Table 2). Among them five cases showed two or three alterations located within a short stretch of nucleotides less than 30 bp long. This could be induced by clustered damage or by locally multiply damaged sites suggested by computer simulation of DNA damage (*37*). The other four multiple mutations displayed two base substitutions at separate positions located more than 500 bp apart. Since these were found only in irradiated *Ku70*-deficient mice, this type of mutation could be related to the NHEJ deficiency. Six out of eight base substitutions found in these multiple mutations were G:C to A:T transitions at CG sequences, a mutation type that is found most frequently in spontaneous mutations in vertebrates. Recently, Wang *et al.* proposed a phenomenon known as "mutation showers" as the cause of multiple mutations, which could occur as a result of a temporally unstable DNA polymerase or an imbalance in the deoxyribonucleotide triphosphate pool size (*38*). The multiple mutations observed in the present study could be explained by the same mechanism, although there is no evidence that Ku70 is involved in DNA polymerization or the maintenance of nucleotide pool levels.

In the present study we examined three tissues with different cell proliferation properties and asked whether there is any tissue specificity in mutation induction. The dose response of mutation induction revealed variation among the tissues, especially at 50 Gy (Fig. 1). The suppression of mutation induction at high doses could be explained by an increased probability of having two events in a single cell: mutation on the *lacZ* gene and a lethal hit for the cell. In fact, the strongest suppression was observed in the spleen, which was the most sensitive tissue among the three tissues examined. Brain cells would be more radioresistant than spleen and liver cells.

In conclusion, in *Ku70*$^{-/-}$ mice, end rejoining of X-ray-induced DNA breaks is impaired due to the absence of NHEJ repair, and the formation of mutations is suppressed. On the other hand, some non-NHEJ mediated DNA rejoining, which could be homologous recombination repair, appears to occur in *Ku70*-deficient animals.

ACKNOWLEDGMENTS

We thank Dr Frederick W. Alt for providing the *Ku70*$^{+/-}$ mice and Yasuko Syono, Yukiko Ikeda and Akemi Miura for technical support. The study was supported by grants from the "Ground-based Research Program for Space Utilization" promoted by the Japan Space Forum, the Budget for Nuclear Research of the Ministry of Education, Culture, Sports, Science and Technology, based on screening and counseling by the Atomic Energy Commission, and the NIFS Collaborative Research Program (NIFS07KOBS012).

Received: November 10, 2007; accepted: March 25, 2008

REFERENCES

1. M. R. Lieber, Y. Ma, U. Pannicke and K. Schwarz, Mechanism and regulation of human non-homologous DNA end-joining. *Nat. Rev. Mol. Cell Biol.* **4**, 712–720 (2003).

2. J. A. Downs and S. P. Jackson, A means to a DNA end: the many roles of Ku. *Nat. Rev. Mol. Cell Biol.* **5**, 367–378 (2004).
3. J. Thacker and M. Z. Zdzienicka, The XRCC genes: expanding roles in DNA double-strand break repair. *DNA Repair* **3**, 1081–1090 (2004).
4. S. Burma, B. P. C. Chen and D. J. Chen, Role of non-homologous end joining (NHEJ) in maintaining genomic integrity. *DNA Repair* **5**, 1042–1048 (2006).
5. D. Buck, L. Malivert, R. de Chasseval, A. Barraud, M-C. Fondanèche, O. Sanal, A. Plebani, J-L. Stéphan, M. Hufnagel and P. Revy, Cernunnos, a novel nonhomologous end-joining factor, is mutated in human immunodeficiency with microcephaly. *Cell* **124**, 287–299 (2006).
6. P. Ahnesorg, P. Smith and S. P. Jackson, XLF interacts with the XRCC4-DNA ligase IV complex to promote DNA nonhomologous end-joining. *Cell* **124**, 301–313 (2006).
7. A. Nijnik, L. Woodbine, C. Marchetti, S. Dawson, T. Lambe, C. Liu, N. P. Rodrigues, T. L. Crockford, E. Cabuy and R. J. Cornall, DNA repair is limiting for haematopoietic stem cells during ageing. *Nature* **447**, 686–693 (2007).
8. D. J. Rossi, D. Bryder, J. Seita, A. Nussenzweig, J. Hoeijmakers and I. L. Weissman, Deficiencies in DNA damage repair limit the function of haematopoietic stem cells with age. *Nature* **447**, 725–729 (2007).
9. Z. E. Karanjawala, U. Grawunder, C-L. Hsieh and M. R. Lieber, The nonhomologous DNA end joining pathway is important for chromosome stability in primary fibroblasts. *Curr. Biol.* **9**, 1501–1506 (1999).
10. D. O. Ferguson, J. M. Sekiguchi, S. Chang, K. M. Frank, Y. Gao, R. A. DePinho and F. W. Alt, The nonhomologous end-joining pathway of DNA repair is required for genomic stability and the suppression of translocations. *Proc. Natl. Acad. Sci. USA* **97**, 6630–6633 (2000).
11. M. J. Difillppantonlo, J. Zhu, H. T. Chen, E. Meffre, M. C. Nussenwig, E. E. Max, T. Ried and A. Nussenzweig, DNA repair protein Ku80 suppresses chromosomal aberrations and malignant transformation. *Nature* **404**, 510–514 (2000).
12. L. D. Rockwood, A. Nussenzweig and S. Janz, Paradoxical decrease in mutant frequencies and chromosomal rearrangements in a transgenic *lacZ* reporter gene in Ku80 null mice deficient in DNA double strand break repair. *Mutat. Res.* **529**, 51–58 (2003).
13. M. Martín, A. Genescà, L. Latre, I. Jaco, G. E. Taccioli, J. Egozcue, M. A. Blasco, G. Iliakis and L. Tusell, Postreplicative joining of DNA double-strand breaks causes genomic instability in DNA-PKcs-deficient mouse. *Cancer Res.* **65**, 10223–10232 (2005).
14. K. Rothkamm, M. Kühne, P. A. Jeggo and M. Löbrich, Radiation-induced genomic rearrangements formed by nonhomologous end-joining of DNA double-strand breaks. *Cancer Res.* **61**, 3886–3893 (2001).
15. Y. Peng, Q. Zhang, H. Nagasawa, R. Okayasu, H. L. Liber and J. S. Bedford, Silencing expression of the catalytic subunit of DNA-dependent protein kinase by small interfering RNA sensitizes human cells for radiation-induced chromosome damage, cell killing, and mutation. *Cancer Res.* **62**, 6400–6404 (2002).
16. T. Zhou and L. F. Povirk, Extreme cytotoxicity and susceptibility to hprt mutagenesis in Ku-deficient xrs-6 cells treated with bleomycin in plateau phase. *Mutagenesis* **20**, 39–44 (2005).
17. T. Ono, H. Ikehata, S. Nakamura, Y. Saito, J. Komura, Y. Hosoi and K. Yamamoto, Molecular nature of mutations induced by a high dose of X-rays in spleen, liver, and brain of the *lacZ*-transgenic mouse. *Environ. Mol. Mutagen.* **34**, 97–105 (1999).
18. K. Masumura, K. Kuniya, T. Kurobe, M. Fukuoka, F. Yatagai and T. Nohmi, Heavy-ion-induced mutations in the gpt delta transgenic mouse: comparison of mutation spectra induced by heavy-ion, X-ray, and γ-ray radiation. *Environ. Mol. Mutagen.* **40**, 207–215 (2002).
19. Y. Gu, S. Jin, Y. Gao, D. T. Weaver and F. W. Alt, Ku70-deficient embryonic stem cells have increased ionizing radiosensitivity, defective DNA end-binding activity, and inability to support V(D)J recombination. *Proc. Natl. Acad. Sci. USA* **94**, 8076–8081 (1997).
20. F. Liang, M. Han, P. J. Romanienko and M. Jasin, Homology-directed repair is a major double-strand break repair pathway in mammalian cells. *Proc. Natl. Acad. Sci. USA* **95**, 5172–5177 (1998).
21. M. Honma, M. Izumi, M. Sakuraba, S. Tadokoro, H. Sakamoto, W. Wang, F. Yatagai and M. Hayashi, Deletion, rearrangement, and gene conversion; genetic consequences of chromosomal double-strand breaks in human cells. *Environ. Mol. Mutagen.* **42**, 288–298 (2003).
22. M. Honma, M. Sakuraba, T. Koizumi, Y. Takashima, H. Sakamoto and M. Hayashi, Non-homologous end-joining for repairing I-SceI-induced DNA double strand breaks in human cells. *DNA Repair* **6**, 781–788 (2007).
23. M. E. T. Dollé, W. K. Snyder, J. A. Gossen, P. H. M. Lohman and J. Vijg, Distinct spectra of somatic mutations accumulated with age in mouse heart and small intestine. *Proc. Natl. Acad. Sci. USA* **97**, 8403–8408 (2000).
24. T. Ono, H. Ikehata, V. P. Pithani, Y. Uehara, Y. Chen, Y. Kinouchi, T. Shimosegawa and Y. Hosoi, Spontaneous mutations in digestive tract of old mice show tissue-specific patterns of genomic instability. *Cancer Res.* **64**, 6919–6923 (2004).
25. T. Ono, H. Ikehata, Y. Uehara and J. Komura, The maintenance of genome integrity is tissue-specific. *Genes Environ.* **28**, 16–22 (2006).
26. K. E. Orii, Y. Lee, N. Kondo and P. J. McKinnon, Selective utilization of nonhomologous end-joining and homologous recombination DNA repair pathways during nervous system development. *Proc. Natl. Acad. Sci. USA* **103**, 10017–10022 (2006).
27. L. Brugmans, R. Kanaar and J. Essers, Analysis of DNA double-strand break repair pathways in mice. *Mutat. Res.* **614**, 95–108 (2007).
28. J. A. Gossen, W. J. F. de Leeuw, C. H. T. Tan, E. C. Zwarthoff, F. Berends, P. H. M. Lohman, D. L. Knook and J. Vijg, Efficient rescue of integrated shuttle vectors from transgenic mice: a model for studying mutations *in vivo*. *Proc. Natl. Acad. Sci. USA* **86**, 7971–7975 (1989).
29. Y. Gu, K. J. Seidl, G. A. Rathbun, C. Zhu, J. P. Manis, N. van der Stoep, L. Davidson, H-L. Cheng and F. W. Alt, Growth retardation and leaky SCID phenotype of Ku70-deficient mice. *Immunity* **7**, 653–665 (1997).
30. F. Wang, Y. Saito, T. Shiomi, S. Yamada, T. Ono and H. Ikehata, Mutation spectrum in UVB-exposed skin epidermis of a mildly-affected Xpg-deficient mouse. *Environ. Mol. Mutagen.* **47**, 107–116 (2006).
31. R. Hirayama, Y. Furusawa, T. Fukawa and K. Ando, Repair kinetics of DNA-DSB induced by X-rays or carbon ions under oxic and hypoxic conditions. *J. Radiat. Res.* **46**, 325–332 (2005).
32. J. Sambrook and D. W. Russell, SDS-polyacrylamide gel electrophoresis of proteins. *In Molecular Cloning- A Laboratory Manual*, 3rd ed. (J. Sambrook and D. W. Russell, Eds.), pp. A8.40–A8.55. Cold Spring Harbor Laboratory Press, Cold Spring Harbor, NY, 2001.
33. K. Rothkamm and M. Löbrich, Evidence for a lack of DNA double-strand break repair in human cells exposed to very low x-ray doses. *Proc. Natl. Acad. Sci. USA* **100**, 5057–5062 (2003).
34. J. F. Ward, DNA damage produced by ionizing radiation in mammalian cells: identities, mechanisms of formation, and reparability. *Prog. Nucleic Acids Res. Mol. Biol.* **35**, 95–125 (1988).
35. B. Stenerlöw, K. H. Karlsson, B. Cooper and B. Rydberg, Measurement of prompt DNA double-strand breaks in mammalian cells without including heat-labile sites: Results for cells deficient in nonhomologous end joining. *Radiat. Res.* **159**, 502–510 (2003).
36. A. Nussenzweig, K. Sokol, P. Burgman, L. Li and G. C. Li, Hypersensitivity of *Ku80*-deficient cell lines and mice to DNA damage: The effects of ionizing radiation on growth, survival, and development. *Proc. Natl. Acad. Sci. USA* **94**, 13588–13593 (1997).
37. H. Nikjoo, P. O'Neill, D. T. Goodhead and M. Terrissol, Computational modelling of low-energy electron-induced DNA damage by early physical and chemical events. *Int. J. Radiat. Biol.* **71**, 467–483 (1997).
38. J. Wang, K. D. Gonzalez, W. A. Scaringe, K. Tsai, N. Liu, D. Gu, W. Li, K. A. Hill and S. S. Sommer, Evidence for mutation showers. *Proc. Natl. Acad. Sci. USA* **104**, 8403–8408 (2007).

THE JOURNAL OF BIOLOGICAL CHEMISTRY VOL. 283, NO. 14, pp. 9071–9079, April 4, 2008

DNA Damage-induced Ubiquitylation of RFC2 Subunit of Replication Factor C Complex*[S]

Received for publication, December 3, 2007, and in revised form, January 18, 2008 Published, JBC Papers in Press, February 1, 2008, DOI 10.1074/jbc.M709835200

Junya Tomida[‡§], Yuji Masuda[¶], Hidekazu Hiroaki[‖], Tomoko Ishikawa[‡], Ihnyoung Song[‡‡], Toshiki Tsurimoto[§§], Satoshi Tateishi[¶¶], Tadahiro Shiomi[‖‖], Yasuhiro Kamei[‡**], Jinhyeong Kim[‡**], Kenji Kamiya[¶], Cyrus Vaziri[‡‡], Haruo Ohmori[§], and Takeshi Todo[‡**1]**

*From the [‡]Radiation Biology Center, Kyoto University, Kyoto 606-8501, Japan, [§]Institute for Virus Research, Kyoto University, Kyoto 606-8507, Japan, [¶]Research Institute for Radiation Biology and Medicine, Hiroshima University, Hiroshima 734-8553, Japan, [‖]Division of Structural Biology, Department of Biotechnology and Molecular Biology, Graduate School of Medicine, Kobe University, Kobe 650-0017, Japan, **Department of Radiation Biology and Medical Genetics, Graduate School of Medicine, Osaka University, Osaka 565-0871, Japan, [‡‡]Department of Genetics and Genomics, Boston University School of Medicine, Boston, Massachusetts 02118, [§§]Department of Biology, School of Science, Kyushu University, Fukuoka 812-8581, Japan, [¶¶]Institute of Molecular Embryology and Genetics, Kumamoto University, Kumamoto 860-0811, Japan, and [‖‖]National Institute of Radiological Science, Chiba 263-8555, Japan*

Many proteins involved in DNA replication and repair undergo post-translational modifications such as phosphorylation and ubiquitylation. Proliferating cell nuclear antigen (PCNA; a homotrimeric protein that encircles double-stranded DNA to function as a sliding clamp for DNA polymerases) is monoubiquitylated by the RAD6-RAD18 complex and further polyubiquitylated by the RAD5-MMS2-UBC13 complex in response to various DNA-damaging agents. PCNA mono- and polyubiquitylation activate an error-prone translesion synthesis pathway and an error-free pathway of damage avoidance, respectively. Here we show that replication factor C (RFC; a heteropentameric protein complex that loads PCNA onto DNA) was also ubiquitylated in a RAD18-dependent manner in cells treated with alkylating agents or H_2O_2. A mutant form of RFC2 with a D228A substitution (corresponding to a yeast Rfc4 mutation that reduces an interaction with replication protein A (RPA), a single-stranded DNA-binding protein) was heavily ubiquitylated in cells even in the absence of DNA damage. Furthermore RFC2 was ubiquitylated by the RAD6-RAD18 complex *in vitro*, and its modification was inhibited in the presence of RPA. The inhibitory effect of RPA on RFC2 ubiquitylation was relatively specific because RAD6-RAD18-mediated ubiquitylation of PCNA was RPA-insensitive. Our findings suggest that RPA plays a regulatory role in DNA damage responses via repression of RFC2 ubiquitylation in human cells.

Cellular DNA is continuously damaged by a vast variety of endogenous and exogenous genotoxicants. When genomic DNA is damaged, cells respond by activation of complex signaling networks that delay cell cycle progression, induce repair of lesions, activate damage tolerance pathways, and trigger apoptosis or senescence (1, 2). It is hypothesized that DNA damage-inducible signaling pathways serve important tumor-suppressive roles and prevent mutations that could lead to malignancy. Various genotoxins elicit different forms of DNA damage and result in distinct signal transduction pathways and biological outcomes. Distal steps of DNA damage-induced checkpoint signaling pathways that result in inhibition of the cell cycle are relatively well understood (3, 4). However, molecular details of proximal signaling events and lesion-specific DNA damage recognition events are less clear.

DNA replication and repair require the coordinated actions of multiple proteins on small regions of DNA. A limited number of proteins serve to coordinate multiple replication and repair events. Some proteins function commonly in DNA replication and repair and frequently have a crucial role in both processes. Three such examples are replication protein A (RPA),[2] proliferating cell nuclear antigen (PCNA), and replication factor C (RFC). RPA was originally identified as a eukaryotic single-stranded DNA-binding protein essential for *in vitro* replication of SV40 DNA (5, 6). PCNA is a trimer of three identical subunits arranged head-to-tail to generate a ringlike structure with a large central cavity for encircling DNA. It is well established that PCNA provides a mobile platform to serve as anchor and processivity factor for DNA polymerases during chromosomal replication (7, 8). PCNA is loaded onto the primer-template junction in an ATP-dependent manner by a multiprotein clamp loader, RFC (9, 10). RFC binds preferentially to double-stranded/single-stranded junctions with a recessed 3′-end, which is the DNA target for PCNA loading.

* This work was supported by grants-in-aid for Scientific Research A and B from the Ministry of Education, Culture, Sports, Science and Technology, Japan (to T. T.) and by National Institutes of Health Grants ES09558 and ES12917 (to C. V.). The costs of publication of this article were defrayed in part by the payment of page charges. This article must therefore be hereby marked "*advertisement*" in accordance with 18 U.S.C. Section 1734 solely to indicate this fact.

[S] The on-line version of this article (available at http://www.jbc.org) contains supplemental Figs. 1–5.

[1] To whom correspondence should be addressed: Dept. of Radiation Biology and Medical Genetics, Graduate School of Medicine, Osaka University, B4, 2-2 Yamada-oka, Suita, Osaka 565-0871, Japan. Fax: 81-6-6879-3819; E-mail: todo@radbio.med.osaka-u.ac.jp.

[2] The abbreviations used are: RPA, replication protein A; PCNA, proliferating cell nuclear antigen; RFC, replication factor C; Pol, polymerase; RLC, RFC-like complex; HA, hemagglutinin; PBS, phosphate-buffered saline; HU, hydroxyurea; MMS, methyl methanesulfonate; Sup, supernatant; E1, ubiquitin-activating enzyme; E2, ubiquitin carrier protein; E3, ubiquitin-protein isopeptide ligase; AP, apurinic/apyrimidinic.

RPA, PCNA, and RFC are key proteins that play central roles in DNA replication, participating in competitive polymerase switching during lagging strand synthesis. The DNA polymerase α-primase complex (Pol α) that synthesizes an RNA-DNA hybrid primer requires contact with RPA to remain stably attached to the primed site. For processive DNA synthesis to follow, Pol α must be replaced by DNA polymerase δ (Pol δ). Replacement of Pol α by Pol δ is initiated by interactions between RFC and RPA that disrupt Pol α-RPA interactions and result in removal of Pol α from DNA. After RFC loads PCNA onto the primed site, Pol δ associates with PCNA by displacing RFC. The switching process is indeed coordinated by RPA via cooperative interactions with PCNA and RFC (11, 12). RPA, RFC, and PCNA also play key roles in DNA repair by interacting with many DNA repair enzymes (13–15). Such interactions are believed to play roles in DNA damage recognition and in recruiting and positioning of DNA repair enzymes.

RFC consists of five different subunits, which are homologous to one another and are members of the AAA^+ family of ATPases (16, 17). The RFC1(p140) subunit is sometimes referred to as the "large subunit" as it contains both N- and C-terminal extensions beyond its region of homology with the four "small" subunits. The four small RFC subunits are designated RFC2(p40), RFC3(p36), RFC4(p37), and RFC5(p38) in mammals. Three protein complexes with resemblance to RFC that are involved in maintaining genome stability have been described recently. These RFC-like complexes (RLCs) share four common small subunits (RFC2–5), and each carries a unique large subunit (RAD17, CTF18, or ELG1) replacing the RFC1. These RLCs are involved in the checkpoint response (RAD17-RFC), sister chromatid cohesion (CTF18-RFC), and maintenance of genome stability (ELG1-RFC) (18, 19).

DNA damage sensors and repair proteins must react in a rapid and efficient manner to execute their functions. Frequently the regulation of these proteins involves post-translational modifications, such as phosphorylation and ubiquitylation, to help modulate the assembly and disassembly of complexes and to assist targeting and the regulation of enzymatic activity in a timely manner. For example, RPA is hyperphosphorylated upon DNA damage or replication stress by several checkpoint kinases (20). Hyperphosphorylation alters RPA-DNA and RPA-protein interactions (15, 21). Recent studies in the DNA repair field have highlighted the expanding role of ubiquitylation in the regulation of diverse DNA repair processes and pathways. One of the most striking examples of how ubiquitylation can affect protein function is that of PCNA in the budding yeast *Saccharomyces cerevisiae*. Following DNA damage, PCNA can be monoubiquitylated or polyubiquitylated on the Lys-164 residue, and each modification results in a different outcome with respect to DNA synthesis and repair (22, 23). Monoubiquitylated PCNA directs translesion synthesis via error-prone DNA polymerases, whereas polyubiquitylated PCNA is associated with an error-free DNA repair pathway (22, 23). Mammalian PCNA also undergoes monoubiquitylation after UV irradiation, and monoubiquitylated PCNA preferentially binds to translesion synthesis polymerases that contain one or two copies of ubiquitin-binding domains (24–27).

In contrast to RPA and PCNA, damage-dependent modification of RFC has not been described. Recent studies have significantly broadened the scope of the role of ubiquitylation to include regulatory functions in DNA repair and damage response pathways. Therefore, in this study we investigated whether the clamp loader RFC is likewise subjected to regulated modification. We examined the modification of all subunits in RFC and RLCs. We demonstrated that RFC2 and RFC4 are ubiquitylated following treatment of cells with alkylating agents. The ubiquitylation was partially dependent on RAD18. Surprisingly RPA inhibited the RAD18-dependent ubiquitylation of RFC2. Our results suggest that RFC regulates the DNA damage response pathway via interaction with RPA and ubiquitylation.

EXPERIMENTAL PROCEDURES

Plasmid Constructs—To generate pCDNA·RFC2(p40)FLAG and pCDNA·RFC2(p40)HA, human p40 coding region was amplified by PCR as an EcoRI-XhoI fragment. The PCR product was inserted into the EcoRI-XhoI site either of pCDNA-C-FLAG or pCDNA-C-HA. To generate pCAGGS·RFC2(p40), the human p40 coding region was amplified by PCR as a SalI-XhoI fragment. The PCR product was inserted into the XhoI site of pCAGGS. pCDNA-C-FLAG and pCDNA-C-HA was constructed by inserting the FLAG or HA epitope into the XhoI-XbaI site of pCDNA3.1. Expression plasmids containing human RFC1-FLAG, human FLAG-RAD17, human FLAG-CTF18, human FLAG-p38, human FLAG-p37, and human FLAG-p36 were constructed by inserting their cDNA described previously (28) into pCDNA3. Although N-terminally and C-terminally tagged forms of each RFC2 subunit were used, the presence of the epitope tag did not affect RFC2 regulation at least in the context of experiments reported in this study. pCAGGS·FLAG-Ubiquitin and pCAGGS·hRAD18 were constructed as described previously (25). The expression plasmids for human RFC and PCNA were described earlier (29, 30), and that for human RPA, p11d-tRPA (31), was a generous gift of Dr. Marc S. Wold (University of Iowa College of Medicine, Iowa City, IA). Mouse E1 expression vector RLC (32, 33) was a generous gift of Dr. Hideyo Yasuda (School of Life Science, Tokyo University of Pharmacy and Life Science, Tokyo, Japan). Human cDNAs for RAD6A and RAD18 amplified from a HeLa cDNA library by PCR introducing a NdeI site at the start codon were cloned together into pET20b(+) (Novagen) as an artificial operon. After cloning the PCR fragments, the nucleotide sequences were verified. All the expression plasmids of PCNA, RPA, RFC, E1, RAD6A, and RAD18 were designed for production of intact proteins without any affinity tags.

Cell Culture and Transfection—293A and HCT116 cells were grown in Dulbecco's modified Eagle's medium supplemented with 10% fetal bovine serum. HCT116 *RAD18*$^{-/-}$ cells were established as described previously (25). Cells were transfected with Lipofectamine Plus (Invitrogen) or Lipofectamine 2000 according to the manufacturer's protocol. 2.4 μg of plasmid DNA was used to transfect each 6-cm plate of cells. Transfected cells were treated with genotoxins 24 h post-transfection.

Genotoxin and Inhibitor Treatments—Asynchronous cell cultures were grown to approximately 80% confluency. For UV

treatment, cells were washed with PBS, and exposed to UV light (254 nm) at a fluence rate of 43 J m^{-2}/s. For genotoxin and inhibitor treatment, hydroxyurea (HU; 1 M in H_2O), aphidicolin (dissolved in Me_2SO), methyl methanesulfonate (MMS; dissolved in Me_2SO), ethyl methanesulfonate (dissolved in Me_2SO), *N*-methyl-*N*′-nitro-*N*-nitrosoguanidine (dissolved in Me_2SO), H_2O_2 (diluted in PBS), mitomycin C, bleomycin (dissolved in H_2O), or camptothecin (dissolved in Me_2SO) was added to the culture media to give a final concentration of 2 mM, 0.025 mM, 0.1–1.7 mM, 20 mM, 0.7 mM, 0.5 mM, 0.01 mM, 0.05 mg/ml, or 20 nM, respectively, and cells were exposed for 8 h unless otherwise stated.

Antibodies—A mouse monoclonal antibody against *Drosophila* RFC40 (anti-dRFC40) was used for probing human RFC2(p40). A hybridoma cell line producing anti-dRFC40 antibody was a kind gift from Dr. Gerald M. Rubin (University of California, Berkeley), and monoclonal antibody was purified as described previously (34). To test whether anti-dRFC40 antibody cross-reacts with human RFC2(p40), an HA epitope-tagged form of hRFC2(p40) was overexpressed in 293A cells by transfection, and cell lysate was recovered 24 h post-transfection and then immunoblotted with either anti-dRFC40 or anti-HA antibody. An anti-dRFC40-reactive protein band migrating at 40 kDa was clearly observed only in extracts from HA-hRFC2(p40)-transfected cells and corresponded to the species detected with an anti-HA antibody (supplemental Fig. 1). Therefore, the anti-dRFC40 antibody recognizes human RFC2(p40). To avoid confusion we refer to the anti-dRFC40 antibody as "anti-RFC2" antibody in this study.

Other commercial antibodies used in this study were: anti-HA (Y-11, Santa Cruz Biotechnology), anti-FLAG (M2, Sigma), anti-RFC1 (H-300, Santa Cruz Biotechnology), anti-RAD17 (H-3, Santa Cruz Biotechnology), anti-tubulin (B-5-1-2, Sigma), anti-histone H3 (6.6.2, Upstate; and ab1791, Abcam), and anti-PCNA (PC10, Oncogene).

Preparation of Cell Lysate and Chromatin Fraction—293A cells in a 3.5- or 6-cm dish were washed twice with ice-cold PBS and then harvested into radioimmune precipitation assay buffer (1× PBS, 1% Nonidet P-40, 0.5% sodium deoxycholate, 0.1% SDS, 1 mM phenylmethylsulfonyl fluoride, 1 mM sodium orthovanadate, and protease inhibitor (Nacalai)). The cell suspensions were incubated for 30 min on ice, and then the Nonidet P-40, 0.1% SDS-insoluble fraction and -soluble fractions were separated by centrifugation. The soluble fraction was used as the supernatant (Sup) fraction. The resultant pellet was washed with radioimmune precipitation assay buffer four times and then sonicated after adding SDS-PAGE loading buffer (7% glycerol, 22% SDS, 50 mM Tris-HCl (pH 6.8), 5% β-mercaptoethanol). The resultant solution was used as the chromatin fraction. We confirmed that there were few contaminations in each Sup and chromatin fraction using anti-tubulin and anti-histone H3 antibodies (supplemental Fig. 2).

SDS-PAGE and Western Blotting—Cell extracts were resolved by electrophoresis by 7.5 or 10% SDS-PAGE. Following transfer onto polyvinylidene difluoride or nitrocellulose filters, the blots were incubated with antibodies, and immunoblots were visualized by enhanced chemiluminescence (ECL, Amersham Biosciences; or DURA, Pierce) according to the manufacturers' instructions.

Immunoprecipitation—Cell extracts were incubated with monoclonal mouse anti-RFC2 (dRFC4(p40)) antibody for 1 h at 4 °C and then with 25 μl of protein A/G-agarose (Santa Cruz Biotechnology). After incubation for overnight at 4 °C, the beads were washed with PBS three times and boiled in Laemmli buffer for 5 min, and the bound proteins were analyzed by electrophoresis and immunoblotting.

Protein Purification—Human RFC, PCNA, and RPA were purified as described previously (29, 30). Mouse E1 was overproduced in insect cells and purified as described previously (35). Human RAD6A-RAD18 complex was overproduced in *Escherichia coli* cells and then purified by column chromatography (phosphocellulose, heparin-Sepharose, Mono Q, and gel filtration) from *E. coli* cell lysate. Protein concentrations were determined by Bio-Rad protein assay kit using bovine serum albumin as the standard. Bovine ubiquitin was purchased from Sigma.

In Vitro Ubiquitylation Assay—The reaction mixture (25 μl) contained 20 mM HEPES-NaOH (pH 7.5), 50 mM NaCl, 0.2 mg/ml bovine serum albumin, 1 mM dithiothreitol, 10 mM $MgCl_2$, 1 mM ATP, 33 fmol of singly primed single-stranded M13 mp18 DNA (30), 1.0 μg (9.1 pmol) of RPA, 86 ng (1.0 pmol as a trimer) of PCNA, 75 ng (260 fmol) of RFC, 100 ng (850 fmol) of mouse E1, 175 ng (2.4 pmol) of RAD6A-RAD18 complex, and 12.5 μg (1460 pmol) of ubiquitin. After incubation at 30 °C for 60 min, reactions were terminated with 2 μl of 300 mM EDTA.

Structural Model Building—Homology modeling of the human clamp loader-clamp complex was performed using MODELLER version 7.7 (36). The homologous structures were defined using the fold recognition server FORTE (37). The atomic coordinate of the clamp-clamp loader complex (Protein Data Bank code 1SXJ) was selected as a template for model building. Before submission to MODELLER, the sequence-structure alignment obtained from FORTE was used. Due to the lack of the template structure, the N-terminal 582 residues of human RFC1 were not modeled. The figures were prepared using MOLMOL (38). Coloring of each RFC subunit and PCNA was according to Fig. 2 in the review by Bowman *et al.* (39).

RESULTS

Specific DNA-damaging Agents Induce Modification of RFC2—To analyze the modification of each subunit of the RFC complex, a FLAG epitope-tagged form of each subunit of RFC and RLCs was expressed in human 293A cells. Transfected cells were treated with UV irradiation, γ-ray, HU, or MMS, and then cell extracts were prepared. The cell extracts were separated into Nonidet P-40-insoluble chromatin fractions and -soluble fractions (Sup). RFC and RLC subunits in each fraction were analyzed by SDS-PAGE and Western blotting (Fig. 1*A*). Following MMS treatment all of the subunits, except for CTF18 and RFC5, accumulated in the chromatin fraction, whereas no accumulation was observed following treatments with UV irradiation, γ-ray, or HU. Levels of soluble CTF18 and RFC5 decreased after MMS treatment, although we did not detect concomitant increases in the chromatin-bound levels of these

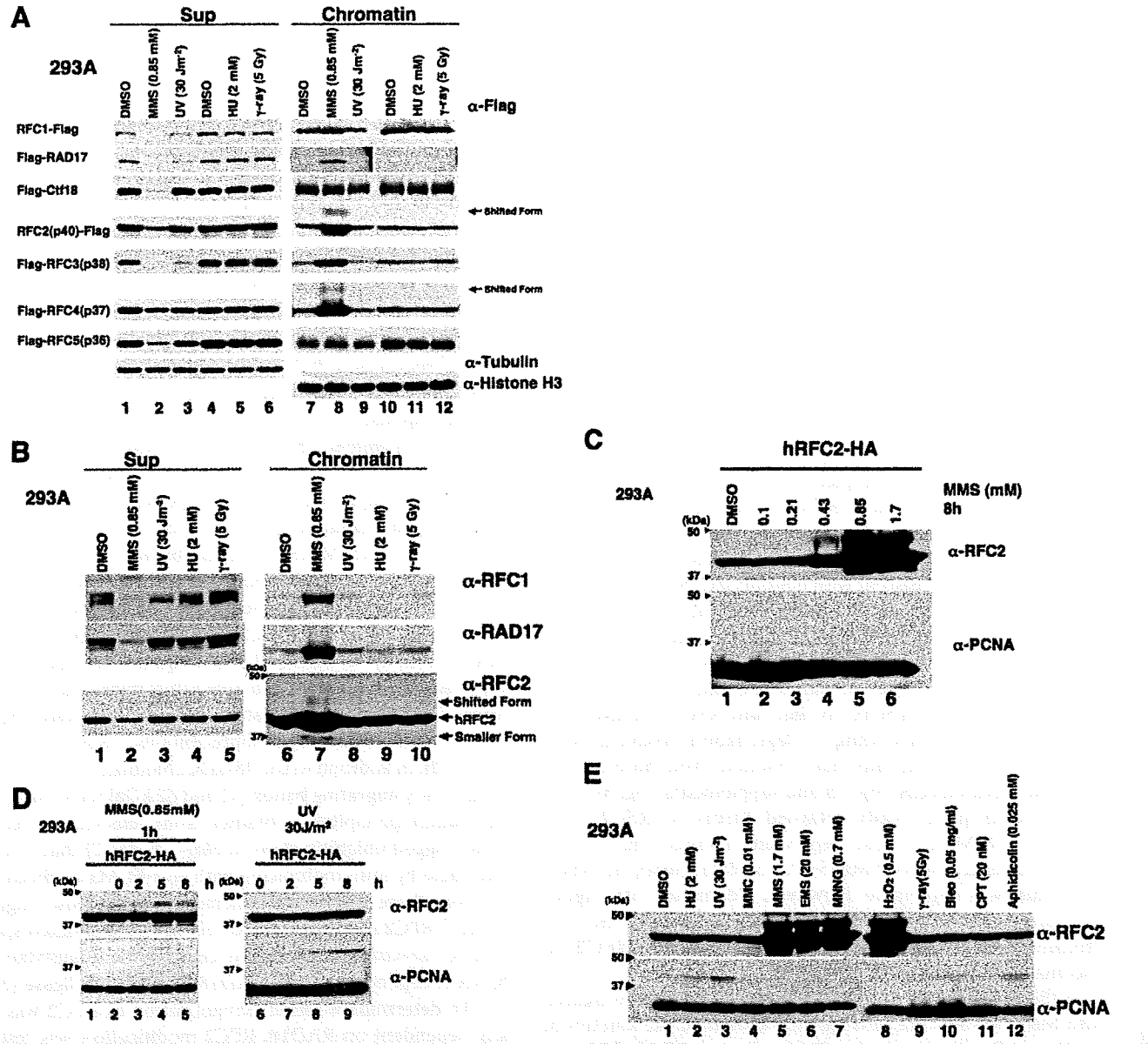

FIGURE 1. **Accumulation of RFC complex in chromatin fraction and modification of RFC2 following treatment of 293A cells with DNA-damaging agents.** *A*, 293A cells transfected with a FLAG epitope-tagged form of each subunit of RFC and RLCs were irradiated with UV light (*lanes 3* and *9*) or γ-ray (*lanes 6* and *12*) or treated with Me_2SO (*DMSO*; *lanes 1*, *4*, *7*, and *10*), MMS (*lanes 2* and *8*), or HU (*lanes 5* and *11*) for 8 h. Cell extracts recovered from transfected cells were then separated into chromatin (*lanes 7–12*) and soluble (*Sup*; *lanes 1–6*) fractions and analyzed by Western blotting with anti-FLAG. Cell extracts recovered from RFC4-transfected cells were also analyzed by Western blotting with anti-tubulin or anti-histone H3 (*lowest two blots*). *B*, 293A cells were irradiated with UV light (*lane 3*) or γ-ray (*lane 5*) or treated with Me_2SO (*lane 1*), MMS (*lane 2*), or HU (*lane 4*) for 8 h. Cell extracts recovered from transfected cells were then separated into chromatin and soluble (*Sup*) fractions and analyzed by Western blotting either with anti-RFC1, anti-RAD17, or anti-RFC2. The *arrowheads* indicate the position of molecular mass markers (kDa). *C*, 293A cells transfected with pCDNA3·RFC2-HA were treated with the indicated dose of MMS for 8 h. Chromatin fractions from the resulting cells were analyzed by immunoblotting with anti-RFC2 or anti-PCNA. The *arrowheads* indicate the position of molecular mass markers (kDa). *D*, 293A cells transfected with pCDNA3·RFC2-HA were treated with 0.85 mM MMS for 1 h (*lanes 2–5*) or UV light-irradiated at 254 nm with 30 J m^{-2} (*lanes 6–9*) and then incubated for the indicated times. Chromatin fractions were prepared and analyzed by Western blotting with anti-RFC2 and anti-PCNA. Cells treated with Me_2SO (*lane 1*) are shown as control. The *arrowheads* indicate the position of molecular mass markers (kDa). *E*, 293A cells transfected with pCDNA3·RFC2-HA were treated with various genotoxic agents. Chromatin fractions were prepared and analyzed by Western blotting with anti-RFC2 or anti-PCNA. The *arrowheads* indicate the position of molecular mass markers (kDa). *Gy*, grays; *MMC*, mitomycin C; *EMS*, ethyl methanesulfonate; *MNNG*, *N*-methyl-*N*′-nitro-*N*-nitrosoguanidine; *Bleo*, bleomycin; *CPT*, camptothecin.

subunits (Fig. 1*A*). Taken together, the results of Fig. 1*A* demonstrate that the levels and subcellular distribution of RFC and RLC subunits are regulated in response to MMS.

It was important to determine whether endogenous RFC and RLC subunits were also redistributed to chromatin in response to MMS. Therefore, we determined the effects of MMS on endogenous RFC1, RAD17, or RFC2 proteins for which good antibodies are available. As shown in Fig. 1*B*, endogenous RFC1, RAD17, and RFC2 accumulated in the chromatin fraction of MMS-treated 293A cells. Similar to

ectopically expressed tagged proteins, endogenous RFC subunits were redistributed to chromatin in response to MMS treatment.

Interestingly we observed prominent forms of ectopically expressed RFC2 and RFC4 that migrated with reduced electrophoretic mobility on SDS-PAGE gels in chromatin fractions from MMS-treated 293A cells (Fig. 1*A*, *lane 7*). Electrophoretically retarded species of endogenous RFC2 were also evident in chromatin fractions of MMS-treated 293A cells (Fig. 1*B*, *lane 7*). The electrophoretically shifted form of RFC2 was more prominent than that of RFC4 (Fig. 1*A*). Therefore we focused on RFC2 and further analyzed its MMS-induced modification.

We performed quantitative analyses to determine the amount of chromatin-bound RFC2 relative to the soluble fraction in MMS-treated cells. In 293A cells ectopically expressing HA-tagged RFC2, more than 90% of the RFC2 accumulated in the chromatin fraction following 8 h of MMS treatment, whereas in untreated cells, less than 10% of RFC2 was present in the chromatin fraction (supplemental Fig. 3). Following MMS treatment, we consistently detected two electrophoretically retarded anti-RFC2-reactive proteins in the chromatin fraction. The apparent molecular mass of electrophoretically retarded RFC2 is consistent with ubiquitylation. The two putative ubiquitylated forms of RFC2 (shown in Fig. 1) might correspond to species that are monoubiquitylated on different residues. However, we cannot exclude the possibility that modifications other than ubiquitin are also present on the shifted RFC2. Furthermore smaller anti-RFC2-reactive proteins, possibly corresponding to degradation products, were detected in soluble and chromatin fractions from both control and MMS-treated cells (Fig. 1*B* and supplemental Fig. 3).

The electrophoretically retarded forms of RFC2 were induced by MMS in a dose-dependent manner (Fig. 1*C*). At lower concentrations of MMS (0.1 or 0.213 mM), no RFC2 band shift was detectable. However, treatment with higher concentrations of MMS (0.425, 0.85, or 1.7 mM) induced prominent electrophoretically retarded forms of RFC2 on chromatin (Fig. 1*C*).

In the experiments described above, the cells were treated with MMS for 8 h. We subsequently examined the kinetics of RFC2 modification by treating 293A cells with MMS (0.85 mM) for 1 h and preparing samples for immunoblotting at 0, 2, 5, and 8 h following MMS treatment. As shown in Fig. 1*D*, the shifted forms of RFC2 were detectable by 5 h after treatment of cells with MMS (*lane 4*). Similar to results of Fig. 1*A*, the genotoxin-induced RFC2 mobility shift was specific for MMS because UV irradiation (30 J/m^2; *lanes 7–9*) did not induce RFC modification at any time point tested (although as expected, UV irradiation induced PCNA monoubiquitylation under these experimental conditions). Conversely little or no PCNA modification was detectable under the conditions used for the experiment shown in Fig. 1*D* (*lanes 2–5*), although low levels of PCNA ubiquitylation were observed when cells were treated with 0.85 mM MMS for longer times (data not shown).

The results of Fig. 1, *A* and *D*, indicated that MMS-induced RFC2 modification is not a general response to DNA damage. To gain insight into the significance of RFC2 modification, 293A cells ectopically expressing RFC2-HA were treated with a more extensive panel of DNA-damaging agents for 8 h, and proteins in resulting chromatin fractions were analyzed by immunoblotting with the anti-RFC2 antibody (Fig. 1*E*, *upper panel*). DNA-damaging agents we tested included alkylating agents (ethyl methanesulfonate and *N*-methyl-*N*′-nitro-*N*-nitrosoguanidine), an oxidizing agent (H_2O_2), a DNA cross-linking agent (mitomycin C), double strand break-inducing agents (bleomycin and ionizing radiation), and the topoisomerase I inhibitor camptothecin. Of the genotoxic agents tested, only ethyl methanesulfonate, *N*-methyl-*N*′-nitro-*N*-nitrosoguanidine, and H_2O_2 induced the shifted RFC2 band evident in MMS-treated cells (Fig. 1*E*, *upper panel, lanes 7–10*). Many of the agents failing to induce the RFC2 band shift nevertheless induced very robust PCNA monoubiquitylation (Fig. 1*E*, *lower panel*). Therefore, we conclude that RFC2 modification is a specific response to a subset of genotoxins.

RAD18-dependent Ubiquitylation of Human RFC2—To test whether the shifted RFC2-specific band in MMS-treated cells was due to ubiquitylation, RFC2-HA was co-expressed with FLAG-tagged ubiquitin in 293A cells. The transfected cells were treated with MMS. Endogenous and HA-tagged RFC2 proteins were immunoprecipitated with anti-RFC2 antibody from cell lysates, and the precipitated proteins were immunoblotted with either anti-RFC2 (Fig. 2*A*, *upper panel*) or anti-FLAG antibody to detect FLAG-ubiquitin-modified proteins (*lower panel*). Anti-RFC2-reactive bands migrating at the sizes expected for monoubiquitylated RFC2 (48 kDa) were observed in our anti-RFC2 immunoprecipitates (*lanes 3* and *4*, *Ub-RFC2*). In addition to the 48-kDa ubiquitin-RFC2 band, two extra, slowly migrating bands (51 and 62 kDa) were observed in the immunoprecipitates obtained from cells transfected with FLAG-tagged ubiquitin (*lane 4*, *Flag-Ub-RFC2*) that were also detectable by immunoblotting with anti-FLAG antibody (*lane 8*). From these results we conclude that the slow migrating forms of RFC2 in MMS-treated cells are ubiquitylated species.

In *S. cerevisiae* and human cells, monoubiquitylation of PCNA is dependent on the RAD18 E3 ubiquitin ligase (22, 24, 25). To determine whether ubiquitylation of RFC2 was similarly dependent on RAD18, RFC2 modification was tested in RAD18-overexpressing 293A cells (Fig. 2*B*) and *RAD18*-deficient HCT116 cells (Fig. 2*C*). As shown in Fig. 2*B*, overexpression of RAD18 induced the ubiquitylation of RFC2-HA and PCNA even in the absence of MMS treatment. Conversely MMS-induced ubiquitylated forms of RFC2 decreased considerably (by 50%) in HCT116 *RAD18*$^{-/-}$ cells compared with those in matched HCT116 *RAD18*$^{+/+}$ cells (Fig. 2*C*). These results suggest that RFC2 monoubiquitylation in MMS-treated cells is mediated at least in large part by RAD18, most probably as a complex with RAD6. Interestingly RAD18 overexpression also induced chromatin accumulation of RFC2 (Fig. 2*B*). Ubiquitylation and chromatin accumulation of RFC2 (and also RFC4) was observed in response to MMS treatment and RAD18 overexpression. Because MMS treatment induced chromatin accumulation of each RFC subunit (Fig. 1*A*), it is most likely that increased chromatin loading of the entire RFC complex occurs in response to MMS.

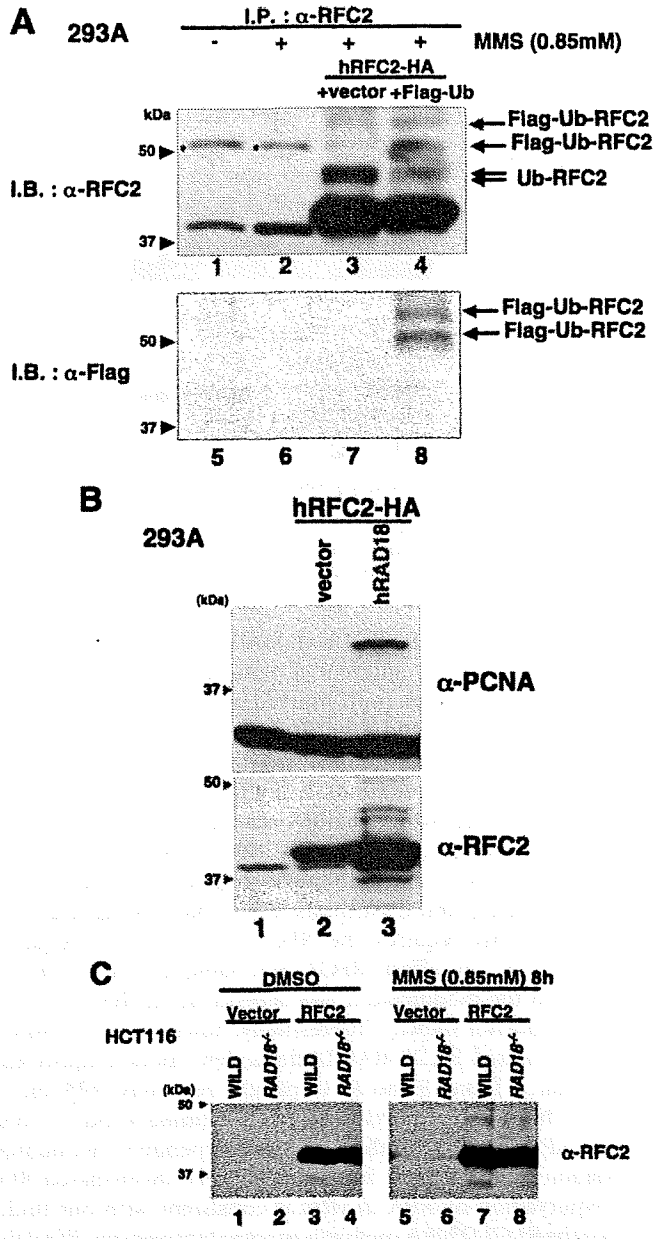

FIGURE 2. **RFC2 monoubiquitylation in response to DNA-damaging agents is RAD18-dependent.** *A*, lysates from RFC2-HA- and FLAG-ubiquitin-co-transfected 293A cells were analyzed by immunoprecipitation and Western blotting. pCDNA3·RFC2-HA was co-transfected either with pCAGGS-FLAG-Ubiquitin (*lanes 4* and *8*) or empty vector (*lanes 3* and *7*) in 293A cells. The following day, cells were treated with MMS for 8 h, and then cell extracts were recovered. Cell extracts were immunoprecipitated with anti-RFC2 antibody. The resulting immune complexes were recovered using protein A/G-agarose and detected by immunoblotting with anti-RFC2 antibody (*lanes 1–4*) or anti-FLAG antibody (*lanes 5–8*). *Asterisks* show nonspecific bands. *B*, Western blot of lysates from 293A cells overexpressing hRAD18. pCDNA3·RFC2-HA was co-transfected either with pCAGGS·hRAD18 (*lane 3*) or empty vector (*lane 2*) in 293A cells. Chromatin fractions were prepared and analyzed by Western blotting with anti-RFC2 (*lower panel*) or anti-PCNA (*upper panel*). The *arrowheads* indicate the position of molecular mass markers (kDa). *C*, Western blot of lysates from HCT116 cells (*WILD*) or *RAD18*-deficient HCT116 cells (*RAD18*$^{-/-}$). HCT116 cells transfected either with empty vector or pCAGGS·hRFC2 were treated with 0.85 mM MMS for 8 h. Chromatin fractions from the resulting cells were analyzed by immunoblotting with anti-RFC2 antibody. The *arrowheads* indicate the position of molecular mass markers (kDa). *I.P.*, immunoprecipitate; *I.B.*, immunoblot; *DMSO*, Me_2SO; *Ub*, ubiquitin.

An RFC2 Mutant Is Ubiquitylated in the Absence of DNA Damage—It has been reported that the RFC2(p40) subunit of human RFC binds the large subunit of RPA (11). In *S. cerevisiae*, a mutation in *rfc4* (yeast homolog of human RFC2(p40)) was found to display synthetic lethality with mutation in the gene encoding Rpa1 (the large subunit of *S. cerevisiae* RPA) (40). Interestingly this mutant Rfc4(p40) showed weaker physical interaction with RPA than did the wild type Rfc4(p40). This mutation, resulting in an amino acid change of aspartate to asparagine at residue 201, maps to the RFC box VIII, which is one of the conserved motifs found in all RFC subunits (16, 41). The Asp-201 residue of *S. cerevisiae* Rfc4 is conserved and found at an identical position in RFC2 from higher eukaryotes, including humans (Fig. 3*A*). We replaced Asp-228 of human RFC2 (which corresponds to *S. cerevisiae* Rfc4 Asp-201) with an asparagine residue (D228N) or an alanine (D228A). HA-tagged forms of mutant or wild-type RFC2 were expressed in 293A cells by transfection (Fig. 3*B*). The wild-type and mutant forms of RFC2-HA were expressed at similar levels; however, whereas the wild-type and D228N mutant RFC2 proteins showed no ubiquitylation of RFC2, the D228A mutant RFC2 protein underwent extensive modification without any genotoxin treatment (Fig. 3*B*, *lane 8*). The multiple shifted bands of RFC2 D228A decreased by 55% in HCT116 *RAD18*$^{-/-}$ cells compared with those in matched HCT116 *RAD18*$^{+/+}$ cells (Fig. 3*C*). Therefore, we conclude that the multiple RAD18-dependent species we observed correspond to mono- and polyubiquitylated forms of RFC2. As described in the previous sections, we observed monoubiquitylated forms of the wild-type RFC2-HA in MMS-treated cells but did not observe high levels of its polyubiquitylated forms. The results of Fig. 3*B* indicate that the RFC2 D228A mutant is extensively ubiquitylated and accumulates as multiple polyubiquitylated species (even in the absence of genotoxin treatments) when ectopically expressed. Although the difference in susceptibility to spontaneous ubiquitylation between D228A and D228N is unexpected, by analogy with the *S. cerevisiae* Rfc4 D201N mutant protein, it is most likely that Asp-228 of human RFC2 is also involved in interaction with RPA. Although we have not formally verified the reduced interaction of human RFC D228A with RPA, we infer that RAD6-RAD18-mediated RFC2 ubiquitylation is regulated by interaction with RPA (see below).

RFC2 Is Modified by the RAD6-RAD18 Complex in Vitro—We subsequently examined whether RFC2 could be modified by the RAD6-RAD18 complex *in vitro*. Recombinant RFC complex (including RFC1–5 proteins of human origin) was expressed in *E. coli* and then purified. Monoubiquitylation of RFC2 *in vitro* was investigated by mixing the RFC1–5 complex with purified recombinant RAD6A (E2 ubiquitin-conjugating enzyme)-RAD18 (E3 ubiquitin ligase) complex. As shown in Fig. 4, RFC2 was monoubiquitylated *in vitro* when incubated in the presence of purified RAD6A and RAD18 plus ubiquitin and its activating enzyme (*lane 2*) although at a much lower efficiency when compared with PCNA. It should also be noted that the *in vitro* modification of RFC2 generated only a single monoubiquitylated species, whereas at least two monoubiquitylated forms of RFC2 (corresponding to monoubiquitylation at

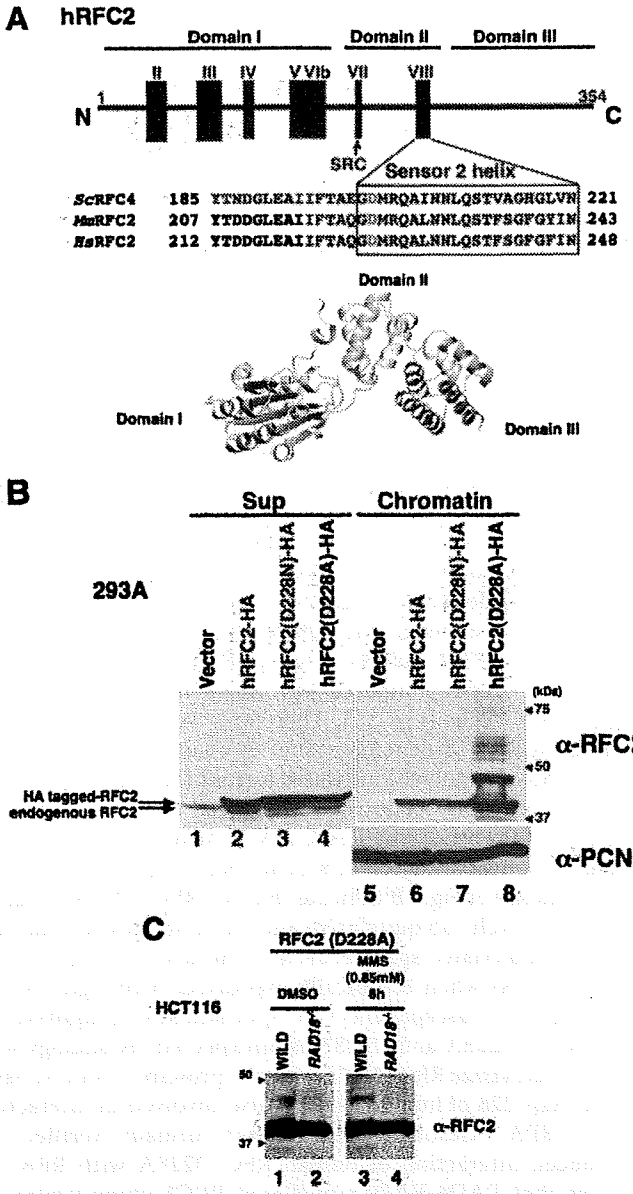

FIGURE 3. **DNA damage-independent monoubiquitylation of hRFC2 D228A.** *A*, schematic diagram and tertiary model of human (*Hs*) RFC2 showing the location of Asp-228 and the sequences of the surrounding regions. Corresponding sequences for *S. cerevisiae* (*Sc*) RFC2(p40) and mouse (*Mm*) RFC2 homologues are also shown. The conserved Sensor 2 helix is represented by a *box*, and the location of the conserved SRC motif is indicated by an *arrow*. Asp-228 of hRFC2, shown in *red*, corresponds to *S. cerevisiae* Asp-201, which shows synthetic lethality with mutation in Rpa-1(*rfa1*-Y29H). There are seven conserved RFC boxes *numbered* consecutively from the N terminus to C terminus. *B*, 293A cells were transfected with expression vectors encoding wild-type (*lanes 2* and *6*), D228N (*lanes 3* and *7*), or D228A (*lanes 4* and *8*) forms of hRFC2-HA. 24 h after transfection cells were harvested and separated into chromatin (*lanes 5–8*) and soluble fractions (*lanes 1–4*) and then immunoblotted with anti-RFC2 or anti-PCNA antibody. The *arrowheads* indicate the position of molecular mass markers (kDa). *C*, Western blot of lysates from HCT116 cells (*WILD*) or *RAD18*-deficient HCT116 cells (*RAD18*$^{-/-}$). HCT116 cells transfected with pCAGGS-hRFC2(Asp-228) were treated with 0.85 mM MMS for 8 h. Chromatin fractions from the resulting cells were analyzed by Western blotting with anti-RFC2 antibody. The *arrowheads* indicate the position of molecular mass markers (kDa). *DMSO*, Me_2SO.

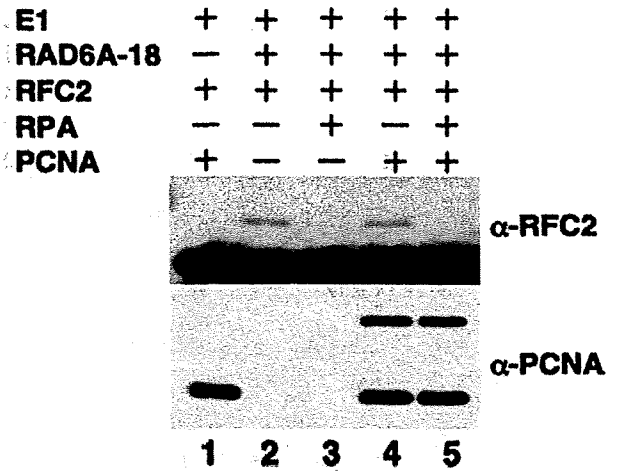

FIGURE 4. ***In vitro* monoubiquitylation of RFC2.** *In vitro* ubiquitylation was carried out by mixing RFC with mouse E1, RAD18-RAD6A complex, ubiquitin, and singly primed single stranded M13 mp18 DNA in the presence or absence of RPA or PCNA as indicated. The reaction products were analyzed by Western blotting with anti-RFC2 or anti-PCNA antibody.

different residues) resulted from MMS treatment of intact cells. The reason for the differential patterns of RAD18-mediated RFC2 monoubiquitylation observed *in vitro* and in intact cells is not yet clear but could result from the existence of additional RFC2-directed E3 ligases *in vivo*. The difference also indicates that *in vitro* assay conditions do not fully recapitulate the complexity of events involved in RPA-sensitive RFC2 ubiquitylation at stalled replication forks *in vivo*. It should be noted that our *in vitro* assay uses primed M13 single-stranded DNA, which mimics the leading strand synthesis rather than the lagging strand synthesis that requires the RFC complex more frequently. PCNA did not affect RFC2 monoubiquitylation (*lane 4*), although the modification was dependent on the presence of DNA (data not shown). Interestingly, however, the addition of RPA inhibited RAD6-RAD18-dependent monoubiquitylation completely (*lanes 3* and *5*). In parallel reactions, RPA did not affect the monoubiquitylation of PCNA (*lanes 4* and *5*). Therefore, RPA specifically inhibits RAD18-dependent monoubiquitylation of RFC2. The inhibition of RAD18-mediated RFC2 ubiquitylation by RPA *in vitro* is consistent with our finding that the RFC2 D228A mutant is more extensively modified than wild-type RFC2 in intact cells.

DISCUSSION

Protein ubiquitylation is critical for numerous cellular functions, including the DNA damage response pathway. In this study we demonstrated that RFC2 is ubiquitylated in human cells via DNA damage-independent and genotoxin-inducible mechanisms. RFC2 ubiquitylation is partially dependent on RAD18 as demonstrated by the decreased MMS-induced RFC2 ubiquitylation in *RAD18*$^{-/-}$ cells compared with matched *RAD18*$^{+/+}$ HCT116 cells (Fig. 2*C*). Conversely RFC2 undergoes genotoxin-independent monoubiquitylation in cells overexpressing RAD18. RAD18-dependent monoubiquitylation of RFC2 was also verified by *in vitro* reaction (Fig. 4). The RAD18-induced ubiquitylation of RFC2 *in vitro* and in RAD18-overexpressing cultured cells is similar to what we and others have

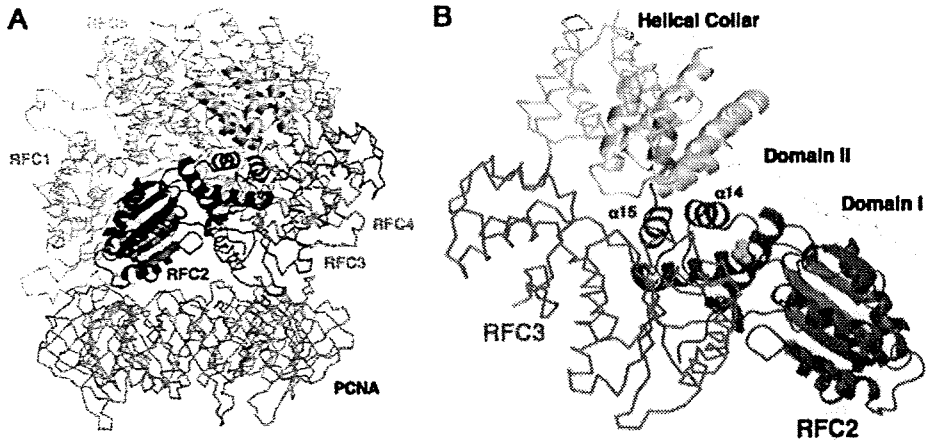

FIGURE 5. **A model for human clamp loader-clamp complex.** Ribbon (RFC2) and wire (Cα trace, RFC1, RFC3–5, and PCNA) representations of the homology model for human RFC1–5-PCNA complex are shown. The five subunits of each clamp loader complex are denoted. The colors for each of the subunits are as follows with the helical collar domains (*gray*) at the top of the figure: *pink*, RFC1; *navy*, RFC2; *red*, RFC3; *green*, RFC4; *orange*, RFC5; *gold*, PCNA. The side chain atoms of Asp-228 of RFC2 are indicated as *balls* in *cyan*. *A*, a side view of the clamp loader-clamp complex in which RFC2 is in the front. *B*, views from the DNA-interacting pore of the clamp loader subunits. Domains I and II of AAA^+ domain and α14 and α15 of RFC2 are indicated.

observed for PCNA, a *bona fide* RAD18 substrate. These results are further indicative of a direct E3 ligase-substrate relationship between RAD18 and RFC2.

Our *in vitro* experiments clearly show an inhibitory effect of RPA on RFC2 monoubiquitylation (Fig. 4). The involvement of RPA in regulation of RFC2 ubiquitylation *in vivo* is also suggested by our experiments with the RFC2 D228A mutant (corresponding to an *S. cerevisiae* RPA interaction-deficient Rfc4 mutant). We have shown that RFC2 D228A underwent DNA damage-independent ubiquitylation, which was reduced substantially in RAD18-deficient cells (Fig. 3*C*). Our *in vitro* assay for RAD6-RAD18-dependent RFC2 ubiquitylation did not completely recapitulate all aspects of RFC2 modification *in vivo*, and the role of RFC2 D228 in mediating RPA associations is not yet clear. However, our results strongly suggest a key regulatory role of RPA in RFC2 ubiquitylation. We propose that RAD18-dependent RFC2 ubiquitylation is repressed by RPA in undamaged cells and that derepression of RFC2 ubiquitylation occurs following MMS-induced DNA damage.

Our experiments also indicate that the RFC2 D228A mutant is subject to extensive polyubiquitylation. It is likely that polyubiquitylated RFC2 is generated by linkage of additional ubiquitin molecules to lysine residues that are first monoubiquitylated by RAD18. By analogy, following genotoxin treatments PCNA is monoubiquitylated by RAD6-RAD18 on lysine 164, and subsequently the monoubiquitylated PCNA is polyubiquitylated in a reaction mediated by MMS2-UBC13 and RAD5 (22, 23, 42, 43). It will be interesting to determine whether RAD5 or alternative E3 ligases contribute to the RAD18-initiated polyubiquitylation of RFC2. Monoubiquitylated and polyubiquitylated species of PCNA promote different damage response pathways, error-prone and error-free postreplication repair, respectively. It will be interesting to determine whether the mono- and polyubiquitylated species of RFC2 similarly serve distinct effector functions. Several studies have demonstrated that a residual level of PCNA ubiquitylation is detectable in RAD18-deficient cells. Similarly we have shown that RAD18-deficiency did not completely ablate RFC2 ubiquitylation. Clearly further work is necessary to identify the E3 ligases involved in RAD18-independent ubiquitylation of PCNA and RFC2.

To obtain insight into the question of why the RFC2 D228A mutant is susceptible to ubiquitylation without DNA damage, we constructed tertiary structure models of human RFC2 (Fig. 3*A*) and RFC complex bound to PCNA (Fig. 5) by homology modeling using the reported yeast structure (41) as the template. Each RFC subunit contains three structurally conserved domains (Domains I, II, and III). Domains I and II comprise an ATPase module of the AAA^+ family that is connected by a flexible linker to another helical domain (Domain III). Our structural model revealed that Asp-228 resides in the turn between helix14 and helix15 (Sensor 2 helix), which is located near the hinge region between Domains II and III (Fig. 5*C*). This implies that RFC2 Asp-228 is not exposed to the outer surface but instead is buried in the spiral structure. It is unlikely, therefore, that the Asp-228 residue directly associates with RPA as long as such a tight RFC-PCNA complex is maintained.

Whether the RFC complex remains around the primed end following PCNA loading is controversial (11, 30, 44–46). However, the RFC complex may stay associated with PCNA in a structure different from the tight complex as shown in Fig. 5*A* that allows RPA to associate with RFC2 around the Asp-228 residue. Another possibility is that the D228A mutation causes a conformational change in the RFC complex structure, possibly altering interactions with RPA and affecting susceptibility to ubiquitylation.

It is notable that RFC2 is ubiquitylated in human cells following treatment with alkylating agents but not in response to genotoxins that induce double strand breaks, bulky adducts, interstrand cross-links, or nucleotide depletion. Therefore, it appears that RFC2 monoubiquitylation is due to a specific alteration in DNA structure induced by alkylating agents or to a specific DNA repair intermediate. Identification of the DNA structure(s) responsible for RFC2 ubiquitylation may provide insight into the consequences of DNA damage due to particular genotoxins. Alkylating agents modify DNA by adding methyl or ethyl groups to a number of nucleophilic sites on the DNA bases (47). The predominant adduct in double strand DNA resulting from MMS or *N*-methyl-*N'*-nitro-*N*-nitrosoguanidine exposure is N^7-methylguanine (N^7-MeG) and N^3-methyladenine (N^3-MeA). N^3-MeA blocks replication, whereas N^7-MeG does not block replication or miscode. Another deleterious adduct is O^6-methylguanine (O^6-MeG). O^6-MeG is produced at a relatively lower level compared with N^7-MeG and N^3-MeA but is highly mutagenic and toxic because O^6-MeG-T mispairing not only results in G/C to A/T transition but also is

recognized by mismatch repair in a process that is a potent signal of apoptosis (48). However, the human kidney cell line 293A cells, which were used in this study, are mismatch repair-deficient due to epigenetic silencing of the *hMLH1* gene by promoter hypermethylation (49). Therefore, O^6-MeG is not the lesion responsible for RFC2 monoubiquitylation, and instead N^7-MeG and/or N^3-MeA are the likely candidates. Treatment of 293A cells with an oxidative agent (H_2O_2) also induced RFC2 monoubiquitylation (Fig. 1*E*). Base excision repair is the common pathway for repairing N^7-MeG, N^3-MeA, and oxidative damage (47, 50, 51). Base excision repair is initiated with removal of altered bases by DNA glycosylase. The resulting apurinic/apyrimidinic (AP) sites are nicked, and repair is completed by resynthesis and ligation. Therefore, for proficient base excision repair, a proper balance of the individual steps involved in DNA repair is important. Imbalanced base excision repair may result in deleterious intermediates, such as AP sites. Furthermore methylation or oxidation of purines destabilizes the *N*-glycosyl bond, thus rendering the base more susceptible to hydrolysis to form an AP site. Therefore, AP sites are the lesions most likely to cause RFC2 monoubiquitylation, although precisely how RPA-RFC2 interaction is affected at AP sites is unclear.

Another possible role of RFC2 ubiquitylation is as the sensing signal for damage recognition. The RFC1–5 complex (containing RFC2) has several functions. During normal DNA replication RFC1–5 acts as clamp loader for PCNA, whereas in the DNA damage response RAD17-RFC2–5 loads the 9-1-1 complex. At present we do not know whether loading of PCNA, the 9-1-1 complex, or both is affected by RAD18-dependent RFC2 modification. Experiments to further address the significance of RFC2 modification and to identify relevant effectors of modified RFC are under way.

Acknowledgments—We greatly appreciate the gift of the expression plasmids for human RPA, p11d-tRPA, from Dr. Marc S. Wold (University of Iowa College of Medicine, Iowa City, IA) and mouse E1 expression vector RLC from Dr. Hideyo Yasuda (School of Life Science, Tokyo University of Pharmacy and Life Science, Tokyo, Japan).

REFERENCES

1. Hartwell, L. H., and Weinert, T. A. (1989) *Science* **246,** 629–634
2. Carr, A. M. (2002) *DNA Repair (Amst.)* **1,** 983–994
3. Kastan, M. B., and Bartek, J. (2004) *Nature* **432,** 316–323
4. Sancar, A., Lindsey-Boltz, L. A., Unsal-Kacmaz, K., and Linn, S. (2004) *Annu. Rev. Biochem.* **73,** 39–85
5. Bochkareva, E., Korolev, S., Lees-Miller, S. P., and Bochkarev, A. (2002) *EMBO J.* **21,** 1855–1863
6. Binz, S. K., Sheehan, A. M., and Wold, M. S. (2004) *DNA Repair (Amst.)* **3,** 1015–1024
7. Kelman, Z., and O'Donnell, M. (1995) *Nucleic Acids Res.* **23,** 3613–3620
8. Wyman, C., and Botchan, M. (1995) *Curr. Biol.* **5,** 334–337
9. Fien, K., and Stillman, B. (1992) *Mol. Cell. Biol.* **12,** 155–163
10. Krishna, T. S., Kong, X. P., Gary, S., Burgers, P. M., and Kuriyan, J. (1994) *Cell* **79,** 1233–1243
11. Yuzhakov, A., Kelman, Z., Hurwitz, J., and O'Donnell, M. (1999) *EMBO J.* **18,** 6189–6199
12. Tsurimoto, T., and Stillman, B. (1991) *J. Biol. Chem.* **266,** 1961–1968
13. Maga, G., and Hubscher, U. (2003) *J. Cell Sci.* **116,** 3051–3060
14. Warbrick, E. (2000) *BioEssays* **22,** 997–1006
15. Zou, Y., Liu, Y., Wu, X., and Shell, S. M. (2006) *J. Cell. Physiol.* **208,** 267–273
16. Cullmann, G., Fien, K., Kobayashi, R., and Stillman, B. (1995) *Mol. Cell. Biol.* **15,** 4661–4671
17. Neuwald, A. F., Aravind, L., Spouge, J. L., and Koonin, E. V. (1999) *Genome Res.* **9,** 27–43
18. Kim, J., and MacNeill, S. A. (2003) *Curr. Biol.* **13,** R873–R875
19. Majka, J., and Burgers, P. M. (2004) *Prog. Nucleic Acids Res. Mol. Biol.* **78,** 227–260
20. Zernik-Kobak, M., Vasunia, K., Connelly, M., Anderson, C. W., and Dixon, K. (1997) *J. Biol. Chem.* **272,** 23896–23904
21. Wu, X., Shell, S. M., and Zou, Y. (2005) *Oncogene* **24,** 4728–4735
22. Hoege, C., Pfander, B., Moldovan, G. L., Pyrowolakis, G., and Jentsch, S. (2002) *Nature* **419,** 135–141
23. Stelter, P., and Ulrich, H. D. (2003) *Nature* **425,** 188–191
24. Kannouche, P. L., Wing, J., and Lehmann, A. R. (2004) *Mol. Cell* **14,** 491–500
25. Watanabe, K., Tateishi, S., Kawasuji, M., Tsurimoto, T., Inoue, H., and Yamaizumi, M. (2004) *EMBO J.* **23,** 3886–3896
26. Friedberg, E. C., Lehmann, A. R., and Fuchs, R. P. (2005) *Mol. Cell* **18,** 499–505
27. Bienko, M., Green, C. M., Crosetto, N., Rudolf, F., Zapart, G., Coull, B., Kannouche, P., Wider, G., Peter, M., Lehmann, A. R., Hofmann, K., and Dikic, I. (2005) *Science* **310,** 1821–1824
28. Shiomi, Y., Shinozaki, A., Nakada, D., Sugimoto, K., Usukura, J., Obuse, C., and Tsurimoto, T. (2002) *Genes Cells* **7,** 861–868
29. Fukuda, K., Morioka, H., Imajou, S., Ikeda, S., Ohtsuka, E., and Tsurimoto, T. (1995) *J. Biol. Chem.* **270,** 22527–22534
30. Masuda, Y., Suzuki, M., Piao, J., Gu, Y., Tsurimoto, T., and Kamiya, K. (2007) *Nucleic Acids Res.* **35,** 6904–6916
31. Henricksen, L. A., Umbricht, C. B., and Wold, M. S. (1994) *J. Biol. Chem.* **269,** 11121–11132
32. Honda, R., Tanaka, H., and Yasuda, H. (1997) *FEBS Lett.* **420,** 25–27
33. Imai, N., Kaneda, S., Nagai, Y., Seno, T., Ayusawa, D., Hanaoka, F., and Yamao, F. (1992) *Gene (Amst.)* **118,** 279–282
34. Harrison, S. D., Solomon, N., and Rubin, G. M. (1995) *Genetics* **139,** 1701–1709
35. Haas, A. L., and Bright, P. M. (1988) *J. Biol. Chem.* **263,** 13258–13267
36. Fiser, A., and Sali, A. (2003) *Methods Enzymol.* **374,** 461–491
37. Tomii, K., and Akiyama, Y. (2004) *Bioinformatics (Oxf.)* **20,** 594–595
38. Koradi, R., Billeter, M., and Wuthrich, K. (1996) *J. Mol. Graph.* **14,** 29–32
39. Bowman, G. D., Goedken, E. R., Kazmirski, S. L., O'Donnell, M., and Kuriyan, J. (2005) *FEBS Lett.* **579,** 863–867
40. Kim, H. S., and Brill, S. J. (2001) *Mol. Cell. Biol.* **21,** 3725–3737
41. Bowman, G. D., O'Donnell, M., and Kuriyan, J. (2004) *Nature* **429,** 724–730
42. Motegi, A., Sood, R., Moinova, H., Markowitz, S. D., Liu, P. P., and Myung, K. (2006) *J. Cell Biol.* **175,** 703–708
43. Unk, I., Hajdu, I., Fatyol, K., Szakal, B., Blastyak, A., Bermudez, V., Hurwitz, J., Prakash, L., Prakash, S., and Haracska, L. (2006) *Proc. Natl. Acad. Sci. U. S. A.* **103,** 18107–18112
44. Gomes, X. V., and Burgers, P. M. (2001) *J. Biol. Chem.* **276,** 34768–34775
45. Podust, V. N., Tiwari, N., Stephan, S., and Fanning, E. (1998) *J. Biol. Chem.* **273,** 31992–31999
46. Moldovan, G. L., Pfander, B., and Jentsch, S. (2007) *Cell* **129,** 665–679
47. Wyatt, M. D., and Pittman, D. L. (2006) *Chem. Res. Toxicol.* **19,** 1580–1594
48. Stojic, L., Brun, R., and Jiricny, J. (2004) *DNA Repair (Amst.)* **3,** 1091–1101
49. Trojan, J., Zeuzem, S., Randolph, A., Hemmerle, C., Brieger, A., Raedle, J., Plotz, G., Jiricny, J., and Marra, G. (2002) *Gastroenterology* **122,** 211–219
50. Hoeijmakers, J. H. (2001) *Nature* **411,** 366–374
51. Krokan, H. E., Nilsen, H., Skorpen, F., Otterlei, M., and Slupphaug, G. (2000) *FEBS Lett.* **476,** 73–77

Published online 20 August 2008

Nucleic Acids Research, 2008, Vol. 36, No. 17 5441–5450
doi:10.1093/nar/gkn516

Biochemical analysis of the N-terminal domain of human RAD54B

Naoyuki Sarai[1,2], Wataru Kagawa[1], Norie Fujikawa[1], Kengo Saito[1,3], Juri Hikiba[3], Kozo Tanaka[4], Kiyoshi Miyagawa[5], Hitoshi Kurumizaka[1,3,*] and Shigeyuki Yokoyama[1,2]

[1]Systems and Structural Biology Center, Yokohama Institute, RIKEN, 1-7-22 Suehiro-cho, Tsurumi, Yokohama 230-0045, [2]Department of Biophysics and Biochemistry, Graduate School of Science, The University of Tokyo, 7-3-1 Hongo, Bunkyo-ku, Tokyo 113-0033, [3]Graduate School of Advanced Science and Engineering, Waseda University, 2-2 Wakamatsu-cho, Shinjuku-ku, Tokyo 162-8480, [4]Institute of Development, Aging and Cancer, Tohoku University, 4-1 Seiryo-machi, Aoba-ku, Sendai 980-8575 and [5]Laboratory of Molecular Radiology, Center of Disease Biology and Integrative Medicine, Graduate School of Medicine, The University of Tokyo, 7-3-1 Hongo, Bunkyo-ku, Tokyo 113-0033, Japan

Received April 25, 2008; Revised July 16, 2008; Accepted July 29, 2008

ABSTRACT

The human RAD54B protein is a paralog of the RAD54 protein, which plays important roles in homologous recombination. RAD54B contains an N-terminal region outside the SWI2/SNF2 domain that shares less conservation with the corresponding region in RAD54. The biochemical roles of this region of RAD54B are not known, although the corresponding region in RAD54 is known to physically interact with RAD51. In the present study, we have biochemically characterized an N-terminal fragment of RAD54B, consisting of amino acid residues 26–225 ($RAD54B_{26-225}$). This fragment formed a stable dimer in solution and bound to branched DNA structures. $RAD54B_{26-225}$ also interacted with DMC1 in both the presence and absence of DNA. Ten DMC1 segments spanning the entire region of the DMC1 sequence were prepared, and two segments, containing amino acid residues 153–214 and 296–340, were found to directly bind to the N-terminal domain of RAD54B. A structural alignment of DMC1 with the *Methanococcus voltae* RadA protein, a homolog of DMC1 in the helical filament form, indicated that these RAD54B-binding sites are located near the ATP-binding site at the monomer–monomer interface in the DMC1 helical filament. Thus, RAD54B binding may affect the quaternary structure of DMC1. These observations suggest that the N-terminal domain of RAD54B plays multiple roles of in homologous recombination.

INTRODUCTION

Homologous recombination is involved in many biologically important processes, and it occurs in all organisms (1–3). In meiosis, homologous recombination is carried out in order to generate genetic diversity, by creating new linkage arrangements between genes or parts of genes. Meiotic recombination also contributes to the establishment of a physical connection between homologous chromosomes, which is essential for proper chromosome segregation (4,5).

Meiotic recombination is initiated by a programed double-strand break (DSB) introduced in the initiation sites for recombination (6). At the DSB site, a single-stranded DNA (ssDNA) tail is produced, and it is incorporated into a protein–DNA complex, called the presynaptic filament. This presynaptic filament catalyzes the homologous pairing and strand-exchange reactions. An intermediate structure, called the Holliday junction, in which two double-stranded DNA (dsDNA) molecules form a four-way junction, is generated through the homologous-pairing and strand-exchange steps. The Holliday junction is then resolved into two DNA molecules by the action of endonucleases.

Studies in the budding yeast *Saccharomyces cerevisiae* initially identified the *rad52* epistasis group of genes (*rad50*, *rad51*, *rad52*, *rad54*, *rdh54/tid1*, *rad55*, *rad57*, *rad59*, *mre11* and *xrs2*) as the core factors of the homologous recombination machinery. The functions of the *rad52* epistasis group genes are highly conserved among eukaryotes, from yeast to human (7,8). One member of this group of genes, *rad54*, encodes a protein that belongs to the SWI2/SNF2 protein family, whose members have

*To whom correspondence should be addressed. Tel: +81 3 5369 7315; Fax: +81 3 5367 2820; Email: kurumizaka@waseda.jp
Correspondence may also be addressed to Shigeyuki Yokoyama. Tel: +81 3 5841 4395; Fax: +81 3 5841 8057; Email: yokoyama@biochem.s.u-tokyo.ac.jp

DNA-dependent ATPase and chromatin-remodeling activities (9–15). Recent studies suggested that Rad54 may play diverse roles in multiple stages of homologous recombination (16,17). Rad54 promotes and stabilizes the Rad51–ssDNA nucleoprotein filament formation by physically interacting with Rad51 (18–21), and it also stimulates the homologous pairing and strand-exchange reactions mediated by Rad51 (22–25). These facts suggest that Rad54 functions in the early stage of homologous recombination. Rad54 is also known to disassemble Rad51 nucleoprotein filaments from DNA, which may be essential in the later stages of recombination (26). Moreover, Rad54 promotes branch migration of the Holliday junction in an ATP-dependent manner, suggesting that Rad54 functions in the late stage of recombination (25).

RAD54B, which shares homology with Rad54, was identified in the human cell as a member of the SWI2/SNF2 family proteins (27). Like Rad54, RAD54B is a DNA-dependent ATPase and stimulates the RAD51-mediated homologous pairing (28,29). Previously, our group and others reported that RAD54B stimulates the recombination activity of DMC1, a meiosis-specific RAD51 homolog, suggesting its role in meiotic homologous recombination (30–32). Therefore, Rad54B may be a paralog of Rad54 having both overlapping and non-overlapping roles with those of Rad54. RAD54B contains helicase motifs, which are commonly found in the members of the SWI2/SNF2 family. Outside this region, RAD54B has an N-terminal region of ~300 amino acid residues. The corresponding region in RAD54 directly interacts with RAD51 (19), suggesting that the N-terminal region of RAD54B may also be essential for the interactions with other recombination factors. However, the N-terminal region of RAD54B is considerably longer than that of RAD54. Hence, it is of interest whether the N-terminal region of RAD54B contains functional regions that are not present in that of RAD54. In the present study, we identified a stable N-terminal domain of the human RAD54B protein, and found that this domain is capable of self-associating, binding to DNA and interacting with both RAD51 and DMC1. These observations suggest multifunctional roles of the N-terminal domain of RAD54B in homologous recombination.

MATERIALS AND METHODS

Purification of RAD54B$_{26-225}$

The His$_6$-tagged human RAD54B$_{26-225}$ protein was overexpressed in the *Escherichia coli* JM109 (DE3) strain carrying an expression vector for the minor tRNAs [Codon(+)RIL, (Novagen, Darmstadt, Germany)], using the pET15b expression system (Novagen). Harvested cells were disrupted by sonication in buffer A (pH 7.8), containing 50 mM Tris–HCl, 0.3 M KCl, 2 mM 2ME, 10% glycerol and 5 mM imidazole. Lysates were mixed gently by the batch method with 4 ml Ni-NTA beads at 4°C for 1 h. The RAD54B$_{26-225}$-coupled Ni-NTA agarose beads were then packed into an Econo-column (Bio-Rad Laboratories, Hercules, CA, USA) and were washed with 30 CV of buffer B (pH 7.8), which contained 50 mM Tris–HCl, 0.3 M KCl, 2 mM 2ME, 10% glycerol and 20 mM imidazole. The His$_6$-tagged RAD54B$_{26-225}$ was eluted in a 30 CV linear gradient of 20–300 mM imidazole in buffer B. RAD54B$_{26-225}$, which eluted in a broad peak, was collected and treated with 2 U of thrombin protease (GE Healthcare, Biosciences, Uppsala, Sweden) per milligram of RAD54B$_{26-225}$. The RAD54B$_{26-225}$ protein was then dialyzed against buffer C (pH 7.2), which contained 20 mM HEPES–KOH, 0.1 M KCl, 0.5 mM EDTA, 2 mM 2ME and 10% glycerol, and was mixed with 2 ml of Benzamidine-Sepharose (GE Healthcare) column matrix at 4°C for 1 h. The proteins in the Benzamidine-Sepharose flow-through fraction were mixed with 8 ml of Q-Sepharose column matrix at 4°C for 1 h. The proteins in the Q-Sepharose flow-through fraction were then mixed with 8 ml of SP-Sepharose column matrix at 4°C for 1 h. The SP-Sepharose column was washed with 20 CV of buffer C, and the RAD54B$_{26-225}$ protein was eluted with a 20 CV linear gradient from 0.1 to 1.0 M KCl in this buffer. The peak fractions of the RAD54B$_{26-225}$ proteins were collected, dialyzed against buffer D (pH 7.5), which contained 20 mM HEPES–KOH, 0.1 M KCl, 0.5 mM EDTA, 2 mM 2ME and 10% glycerol, and stored at −80°C.

Purification of the DMC1 deletion mutants

Ten overlapping glutathione *S*-transferase (GST)-fused DMC1 deletion mutants, composed of amino acid residues 1–44, 24–66, 47–104, 84–126, 118–162, 153–214, 195–237, 225–270, 264–306 and 296–340, respectively, were overexpressed in the *E. coli* JM109 (DE3) strain carrying an expression vector for the minor tRNAs [Codon(+)RIL], using the pET41b expression system (Novagen). The cells were suspended in buffer E (pH 8.0), containing 50 mM Tris–HCl, 0.3 M KCl, 2 mM 2ME, 5 mM EDTA and 10% glycerol, and were disrupted by sonication. Lysates were mixed gently by the batch method with 500 µl Glutathione Sepharose 4B (GS4B) beads (GE Healthcare) at 4°C for 1 h. The beads bound with the GST–DMC1 deletion mutants were then washed four times with 10 ml of buffer E. The GST–DMC1 deletion mutants were eluted by 1 ml of buffer E with 20 mM glutathione. These proteins were dialyzed against buffer E and were stored at 4°C.

The RAD51 and DMC1 proteins were purified as described previously (30,33,34). The concentrations of the purified proteins were determined with a Bio-Rad protein assay kit, using BSA as the standard.

DNA substrates

The ϕX174 circular ssDNA and replicative form I DNA were purchased from New England Biolabs, Ipswich, MA, USA and Life Technologies, Gaithersburg, MD, USA. The concentrations of these DNA are expressed as molar nucleotide concentrations. The oligonucleotides used in this study are shown in Table 1. They were purchased from Invitrogen, Carlsbad, CA, USA, in the desalted form, and were purified by anion exchange

Table 1. Oligonucleotides used in this study

Name	Length	Sequence (5′ to 3′)
PolyA	44-mer	AAAAAAAAAAAAAAAAAAAAAAAAAAAAAAAAAAAAAAAAAAAA
2	50-mer	TGGGTCAACGTGGGCAAAGATGTCCTAGCAATGTAATCGTCTATGACGTT
2a	50-mer	AACGTCATAGACGATTACATTGCTAGGACATCTTTGCCCACGTTGACCCA
5	50-mer	TGCCGAATTCTACCAGTGCCAGTGATGGACATCTTTGCCCACGTTGACCC
6	50-mer	GTCGGATCCTCTAGACAGCTCCATGATCACTGGCACTGGTAGAATTCGGC
7	50-mer	CAACGTCATAGACGATTACATTGCTACATGGAGCTGTCTAGAGGATCCGA
8	51-mer	CAACGTCATAGACGATTACATTGCTAATCACTGGCACTGGTAGAATTCGGC
10	24-mer	GGACATCTTTGCCCACGTTGACCC
15	26-mer	TGCCGAATTCTACCAGTGCCAGTGAT

chromatography. Briefly, the oligonucleotides were dissolved in water and applied to a MonoQ column (GE Healthcare) equilibrated with 10 mM NaOH. Oligonucleotides 2, 2a, 5, 6, 7 and 8 were eluted in a two-step linear gradient, consisting of 5 column volumes of 0–0.6 M NaCl followed by 50 column volumes of 0.6–0.9 M NaCl. Oligonucleotides 10 and 15 were also eluted in a two-step linear gradient, consisting of 5 column volumes of 0–0.5 M NaCl followed by 50 column volumes of 0.5–0.8 M NaCl. Peak fractions were collected, ethanol precipitated and dissolved in water. The substrates with various structures were made by annealing appropriate combinations of oligonucleotides, as described previously (35–37). The combinations of oligonucleotides were as follows: dsDNA, oligonucleotides 2 and 2a; Splayed arm, oligonucleotides 2 and 8; 3′-tailed duplex, oligonucleotides 2 and 10; 5′-tailed duplex, oligonucleotides 8 and 15; 3′-flapped DNA, oligonucleotides 2, 8 and 10; 5′-flapped DNA, oligonucleotides 2, 8 and 15; 3′-PX junction, oligonucleotides 2, 6, 7 and 10; 5′-PX junction, oligonucleotides 2, 6, 7 and 15; and X junction, oligonucleotides 2, 5–7. Oligonucleotide substrates are expressed as molar molecule concentrations.

Gel filtration analysis of $RAD54B_{26-225}$

$RAD54B_{26-225}$ was concentrated to 5.6 mg/ml and 50 µl of the concentrated protein was fractionated through a 25 ml Superdex 200 10/30 GL column (GE Healthcare) using buffer G.

DNA-binding assays of $RAD54B_{26-225}$

For the plasmid DNA-binding assay, the indicated amounts of $RAD54B_{26-225}$ were incubated with ϕX174 ssDNA (20 µM) or ϕX174 dsDNA (10 µM) at 37°C for 20 min in 10 µl of buffer H, containing 50 mM Tris–HCl (pH 7.8), 100 µg/ml BSA and 1 mM DTT. After 10-fold loading dye was added, the products were resolved by 1% agarose gel electrophoresis in TAE buffer at 3.3 V/cm for 2.5 h, and were visualized by staining with ethidium bromide. For the binding assays using oligonucleotide substrates, the indicated amounts of $RAD54B_{26-225}$ were incubated with the DNA substrates (0.2 µM) at 37°C in 10 µl of buffer H for either 10 min for ssDNA or 20 min for other substrates. $A^{32}P$-labeled polyA oligonucleotide was used as the ssDNA substrate, and the resulting $RAD54B_{26-225}$–polyA complex was resolved by 1% agarose gel electrophoresis in 0.5 × TBE buffer at 3.3 V/cm for 2 h. The gel was dried, exposed to an imaging plate and visualized using a BAS2500 image analyzer (Fuji Film Co., Tokyo, Japan). For other DNA substrates containing various structures, the complexes with $RAD54B_{26-225}$ were resolved by 5% polyacrylamide gel electrophoresis in 1 × TBE buffer at 100 V for 50 min, and were visualized by staining with ethidium bromide.

Protein–protein binding assay of $RAD54B_{26-225}$

$RAD54B_{26-225}$ was covalently conjugated to Affi-Gel 15 beads (100 µl, Bio-Rad), according to the manufacturer's instructions. The unbound proteins were removed by washing the beads five times with binding buffer F (pH 7.5), which contained 20 mM HEPES–KOH, 0.15 M KCl, 0.5 mM EDTA, 2 mM 2ME, 10% glycerol and 0.05% Triton X-100. To block the residual active ester sites, ethanolamine (pH 8.0) was added to a final concentration of 100 mM and the resin was incubated at 4°C overnight. After washing the resin five times with 500 µl of buffer F, the Affi-Gel 15-protein matrices were adjusted to 50% slurries with buffer F and were stored at 4°C. For the binding assay, 20 µl of the Affi-Gel 15-protein slurry were mixed with 20 µg of RAD51, DMC1 or RecA at room temperature for 2 h. The Affi-Gel 15-protein beads were then washed five times with 500 µl of buffer F. SDS–PAGE sample buffer (2-fold) was mixed directly with the washed beads. After heating the mixture at 98°C for 5 min, the proteins were fractionated by 12% SDS–PAGE. Bands were visualized by Coomassie Brilliant Blue staining.

In the GS4B pull-down assay, GS4B beads (30 µl) were equilibrated with buffer G, containing 20 mM Tris–HCl (pH 8.0), 0.2 M KCl, 2 mM 2ME, 5 mM EDTA, 10% glycerol and 0.1% NP-40, and were mixed with 10 µg of the GST–DMC1 deletion mutants at 4°C for 30 min. To prevent nonspecific interactions between $RAD54B_{26-225}$ and the GS4B beads, the GS4B–DMC1 deletion mutants were first incubated with 500 µg/ml BSA, and the reaction was incubated at 4°C for 30 min, followed by the addition of 10 µg of $RAD54B_{26-225}$. After an incubation at 4°C for 1 h, the GS4Bbeads were washed with buffer G five times and were eluted with SDS–PAGE sample buffer.

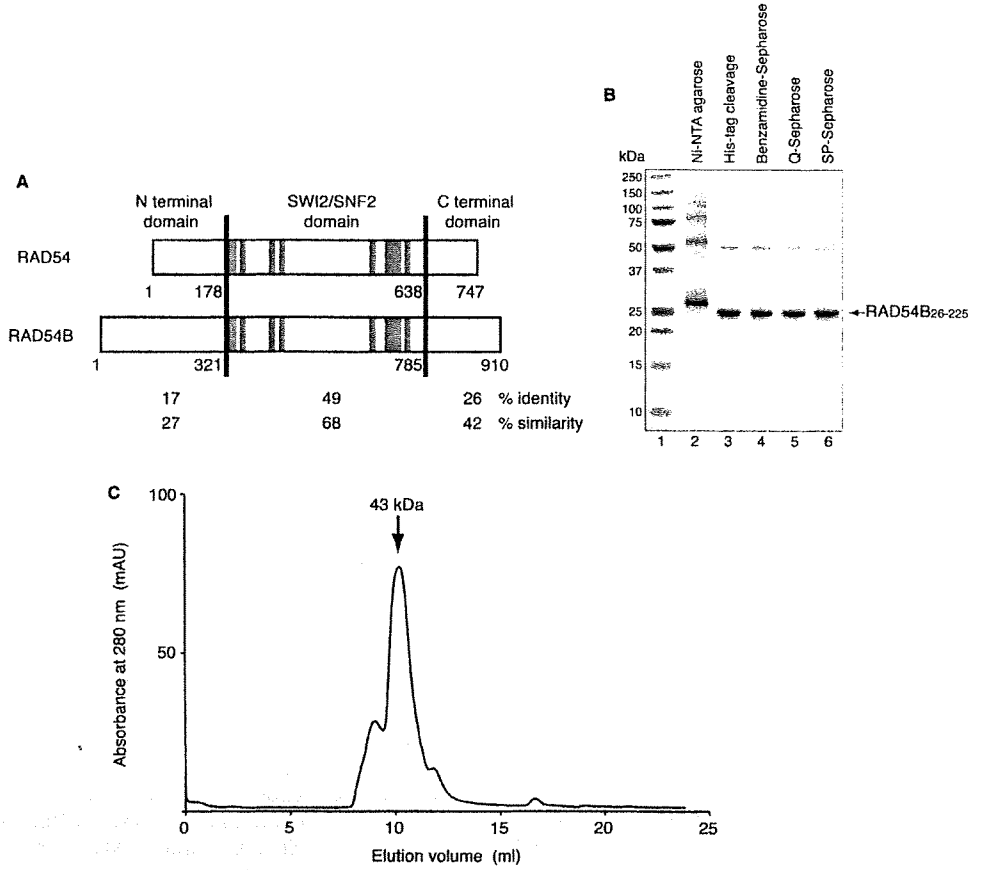

Figure 1. (**A**) Sequence comparison of RAD54 and RAD54B. These proteins are separated into three regions (N-terminal domain, SWI2/SNF2 domain and C-terminal domain), and the amino acid sequence identities and similarities between these proteins were calculated for each region. The amino acid number at the boundary of each domain is denoted. The gray lines indicate the seven helicase motifs (I, Ia, II, III, IV, V and VI, respectively). (**B**) Purification of the $RAD54B_{26-225}$ protein. The peak fractions from the Ni-NTA agarose column (lane 2), the fraction after the removal of the His_6 tag (lane 3), the Benzamidine Sepharose flow-through (lane 4), the Q-Sepharose flow-through (lane 5) and the peak fractions from the SP-Sepharose column (lane 6) were analyzed on a 12% SDS–PAGE gel, which was stained with Coomassie Brilliant Blue. Lane 1 indicates the molecular mass markers. (**C**) Gel filtration analysis of $RAD54B_{26-225}$. The arrow indicates the peak location of a molecular weight marker, ovalbumin (43 kDa), which nearly corresponds to that of $RAD54B_{26\ 225}$.

ssDNA- and dsDNA-binding assays of DMC1

The indicated amounts of DMC1 were incubated with ϕX174 ssDNA (20 μM) or ϕX174 dsDNA (10 μM) at 37°C for 20 min in 10 μl of buffer I, containing 50 mM Tris–HCl (pH 7.8), 1 mM ATP, 2 mM $MgCl_2$, 100 μg/ml BSA and 1 mM DTT. After 10-fold loading dye was added, the products were resolved by 1% agarose gel electrophoresis in TAE buffer at 3.3 V/cm for 2.5 h, and were visualized by staining with ethidium bromide.

Interaction between DMC1 and $RAD54B_{26-225}$ on ssDNA and dsDNA

The reactions were started by incubating 40 μM DMC1 with 20 μM ϕX174 ssDNA or 10 μM ϕX174 dsDNA at 37°C for 20 min, in 10 μl of buffer I. The indicated amounts of $RAD54B_{26-225}$ were then incorporated, and the mixtures were incubated at 37°C for 20 min. After 10-fold loading dye was added, the products were resolved by 1% agarose gel electrophoresis in TAE buffer at 3.3 V/cm for 2.5 h. To determine whether DMC1 was present, the protein–DNA complex was localized by ethidium bromide staining of the agarose gel, and the corresponding area of the gel was excised for electroelution. The eluted proteins were fractionated by 12% SDS–PAGE, and the bands were visualized by Coomassie Brilliant Blue staining.

RESULTS

Purification of the RAD54B N-terminal domain fragment

To gain insight into the function of the N-terminal region of RAD54B, which is less conserved between RAD54 and RAD54B (Figure 1A), we constructed a RAD54B deletion mutant containing the first 295 residues ($RAD54B_{1-295}$).

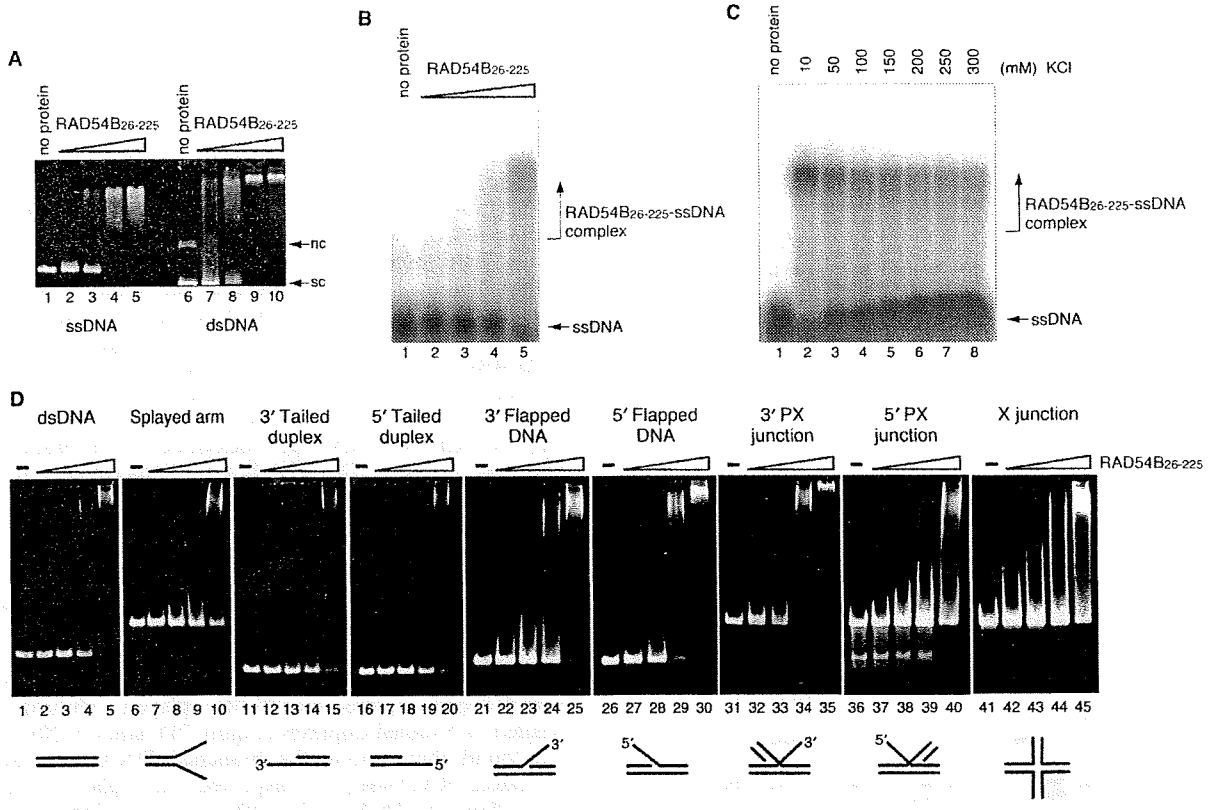

Figure 2. DNA-binding activity of $RAD54B_{26-225}$. (**A**) Plasmid ssDNA (20 μM in nucleotides, lanes 1–5) or plasmid superhelical dsDNA (10 μM in nucleotides, lanes 6–10) was incubated with $RAD54B_{26-225}$ at 37°C for 20 min. The concentrations of $Rad54B_{26-225}$ used in the DNA-binding experiments were 2.0 μM (lanes 2 and 7), 4.0 μM (lanes 3 and 8), 8.0 μM (lanes 4 and 9) and 16 μM (lanes 5 and 10). The reaction mixtures were fractionated on a 1% agarose gel, which was stained with ethidium bromide. Nc and sc indicate nicked circular and superhelical dsDNA, respectively. (**B**) A ^{32}P labeled single-stranded oligonucleotide (polyA 44-mer, 0.2 μM in molecules) was incubated with $RAD54B_{26-225}$ (2, 4, 8 or 16 μM) at 37°C for 10 min and the reaction mixtures were fractionated on a 1% agarose gel. (**C**) Salt concentration titration for the $RAD54B_{26-225}$–polyA complex. $RAD54B_{26-225}$ (16 μM) was incubated with a ^{32}P labeled single-stranded oligonucleotide (polyA 44-mer, 0.2 μM in molecules) in the reaction mixture containing the indicated concentrations of KCl. The reaction mixtures were fractionated on a 1% agarose gel. (**D**) Various branched DNA substrates (0.2 μM in molecules) were incubated with $RAD54B_{26-225}$ (2, 4, 8 or 16 μM) at 37°C for 20 min, and the reaction mixtures were fractionated on a 5% polyacrylamide gel, which was stained with ethidium bromide.

However, this fragment rapidly degraded to several smaller fragments during the expression and purification processes, suggesting that the fragment contained unstructured or flexible regions. Several rounds of fragment design and purification were performed to identify the stable N-terminal region of RAD54B. We found that the fragment consisting of amino acid residues 26–225 of RAD54B ($RAD54B_{26-225}$) was resistant to proteolysis and was highly soluble. The $RAD54B_{26-225}$ mutant was expressed in the *E. coli* JM109 (DE3) strain, as a fusion protein with an N-terminal His_6 tag containing a cleavage site for thrombin protease, and was purified by Ni-NTA column chromatography (Figure 1B, lane 2). After the His_6 tag was uncoupled with thrombin protease (Figure 1B, lane 3), the peak fractions containing $RAD54B_{26-225}$ were further purified by Benzamidine column chromatography (Figure 1B, lane 4), Q-Sepharose column chromatography (Figure 1B, lane 5) and SP-Sepharose column chromatography (Figure 1B, lane 6). About 10 mg of purified $RAD54B_{26-225}$ were obtained from 2.5 l of *E. coli* suspension culture. The SDS–PAGE analysis of the final purification fraction revealed an additional band with an apparent molecular weight of about 50 kDa. The band disappeared when higher concentrations of reducing agent were included in the electrophoresis sample buffer, indicating that $RAD54B_{26-225}$ oligomerizes. Consistent with this observation, a gel filtration analysis of the purified $RAD54B_{26-225}$ indicated that the fragment primarily exists as a dimer (Figure 1C). These results demonstrated that amino acid residues 26–225 of RAD54B form a stable domain. Although it is not known whether the full-length RAD54B protein multimerizes, the N-terminal region may play a role in the self-association of RAD54B.

DNA-binding activity of $RAD54B_{26-225}$

The conserved region of RAD54B (amino acid residues 321–785) contains the helicase motifs involved in DNA binding. As expected, the full-length RAD54B has both

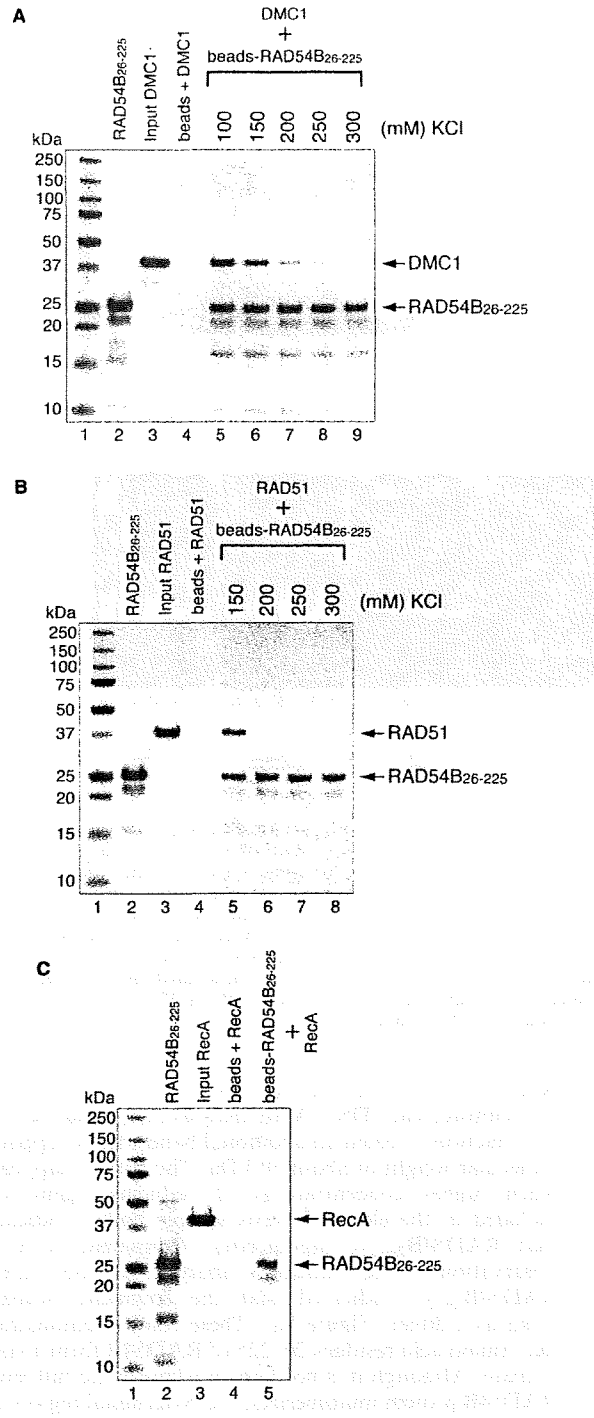

Figure 3. $RAD54B_{26-225}$ interacts with RAD51 and DMC1. The interactions were observed by a pull-down assay, in which DMC1 (**A**) or RAD51 (**B**) was mixed with $RAD54B_{26-225}$ that was covalently conjugated to an Affi-Gel 15 matrix. The proteins bound to the $RAD54B_{26-225}$-conjugated beads were eluted by SDS–PAGE sample buffer, and fractionated on a 12% SDS–PAGE gel. Lanes 2 and 3 are one-tenth of the total proteins used. Lane 4 is the negative control using the Affi-Gel 15 matrix without $RAD54B_{26-225}$. The salt concentration was titrated for both binding experiments, which are shown beyond lane 5. (**C**) Interaction between bacterial RecA and $RAD54B_{26-225}$. The binding experiment was performed in the presence of 100 mM KCl. The bands were visualized by Coomassie Brilliant Blue staining.

ssDNA- and dsDNA-binding activities (28). In contrast, the less conserved N-terminal domain of RAD54B has no known DNA-binding motifs, and it is not known whether this domain binds to DNA. Therefore, we first examined the DNA-binding activity of $RAD54B_{26-225}$, using plasmid ssDNA and dsDNA substrates. As shown in Figure 2A, $RAD54B_{26-225}$ bound to both plasmid ssDNA and dsDNA. To further characterize the DNA-binding activity of $RAD54B_{26-225}$, oligonucleotide substrates were used. $RAD54B_{26-225}$ bound to a polyA ssDNA oligonucleotide, a substrate that is free of secondary structures (Figure 2B). The binding was observed at higher salt concentrations (Figure 2C), suggesting that $RAD54B_{26-225}$ interacts with ssDNA through specific interactions and not by nonspecific ionic interactions. $RAD54B_{26-225}$ also interacted with a dsDNA oligonucleotide, as well as DNA oligonucleotides with branched structures (Figure 2D). The binding experiments were performed using the same concentrations of the DNA substrates (0.2 μM) and RAD54B (2, 4, 8 and 16 μM), to facilitate comparisons between the results with different DNA substrates. We found that $RAD54B_{26-225}$ exhibited slightly higher affinity for dsDNA than ssDNA (compare the amount of uncomplexed DNA between Figure 2B, lane 5 and 2D, lane 5). This was also apparent from the higher affinity for dsDNA than for DNA substrates with shorter duplex regions, such as the splayed arm and the 3′-tailed or 5′-tailed duplexes (Figure 2D, lanes 1–20). We also found that among the branched DNA substrates we tested, $RAD54B_{26-225}$ displayed the highest affinity for 5′-flapped DNA and 3′-PX junction (Figure 2D, lanes 26–35). These results suggested that $RAD54B_{26-225}$ may specifically function on branched DNA molecules.

$RAD54B_{26-225}$ interacts with both RAD51 and DMC1

We have previously shown that RAD54B interacts with RAD51 and DMC1 (30). However, it is not known whether the N-terminal domain of RAD54B is involved in the interactions. We therefore tested the interactions between the N-terminal domain of RAD54B and RAD51 or DMC1 by a pull-down assay, using $RAD54B_{26-225}$-conjugated Affi-Gel 15 beads. The proteins bound to the $RAD54B_{26-225}$ beads were detected by SDS–PAGE. Consistent with the fact that $RAD54B_{26-225}$ self-associates (Figure 1C), we observed $RAD54B_{26-225}$ in the elution fraction that was not covalently conjugated to the Affi-Gel beads (Figure 3A, lanes 5–9; 3B, lanes 5–8 and 3C, lane 5). As shown in Figures 3A and B, $RAD54B_{26-225}$ interacted with both RAD51 and DMC1 (Figure 3A, lanes 5–9 and 3B, lanes 5 and 6, respectively). In contrast, $RAD54B_{26-225}$ weakly bound to RecA, the bacterial homolog of RAD51 and DMC1, suggesting that the interactions between $RAD54B_{26-225}$ and RAD51 or DMC1 were specific (Figure 3C). When the salt concentrations